The developmental changes in intrinsic and synaptic properties of prefrontal neurons enhance local network activity from the second to the third postnatal week in mice

Katerina Kalemaki[1,2], Angeliki Velli[2,3], Ourania Christodoulou[3,4], Myrto Denaxa[4], Domna Karagogeos[1, 2#,*] and Kyriaki Sidiropoulou[2,3#,*]

[1]Department of Basic Science, Faculty of Medicine, University of Crete, Heraklion, Greece

[2]Institute of Molecular Biology and Biotechnology (IMBB), FORTH, Heraklion, Greece

[3]Department of Biology, University of Crete, Heraklion, Greece

[4]BSRC 'Alexander Fleming'

[*] co-corresponding author

[#] equal senior contribution

Abstract

The prefrontal cortex (PFC) is characterized by protracted maturation. The cellular mechanisms controlling the early development of prefrontal circuits are still largely unknown. Our study delineates the developmental cellular processes in the mouse medial PFC (mPFC) during the second and third postnatal weeks and characterizes their contribution to the changes in network activity. We show that spontaneous inhibitory postsynaptic currents (sIPSC) are increased while spontaneous excitatory postsynaptic currents (sEPSC) are reduced from the second to the third postnatal week. Drug application suggested that the increased sEPSC frequency in mPFC at P10 is due to depolarizing $GABA_A$ receptor ($GABA_AR$) function. To further validate this, perforated patch-clamp recordings were obtained and the expression levels of K-Cl co-transporter 2 (KCC2) protein were examined. The reversal potential of IPSCs in response to current stimulation was significantly more depolarized at P10 compared to P20 while KCC2 expression is decreased. Moreover, the number of parvalbumin-expressing GABAergic interneurons increase from P10 to P20 in the mPFC and their intrinsic electrophysiological properties significantly mature. Using computational modeling, we show that the developmental changes in synaptic and intrinsic properties of mPFC neurons contribute to the enhanced network activity in the juvenile compared to neonatal mPFC.

Abbreviations

BC: Barrel Cortex

INs: Interneurons

KCC2: K-Cl co-transporter 2

NKCC1: Na^+-K^+-Cl^- cotransporter 1

mPFC: medial Prefrontal Cortex

P10: Postnatal day 10

P20: Postnatal day 20

PNs: Pyramidal neurons

sEPSC: spontaneous excitatory postsynaptic current

sIPSC: spontaneous inhibitory postsynaptic current

YFP: yellow fluorescent protein

PV: parvalbumin

SST: somatostatin

Introduction

During early postnatal development, major events that contribute to cortical circuit maturation include spatial and temporal patterns of electrical activity, intrinsically determined cell death of early postnatal cortical interneurons and the depolarizing action of the neurotransmitter GABA (γ-aminobutyric acid) (Khazipov et al. 2004; Khazipov and Luhmann 2006; Allene et al. 2008; Brockmann et al. 2011; Ben-Ari et al. 2012; Southwell et al. 2012; Khazipov et al. 2013; Kirmse et al. 2015; Mòdol et al. 2019). The developmental switch of GABA action from depolarizing to hyperpolarizing results from changes in chloride co-transporter expression: Na^+-K^+-Cl^- cotransporter 1 (NKCC1), the Cl^- importer, is highly expressed early in development, while the expression of the co-transporter KCC2, the Cl^- exporter, increases after the first postnatal week (Ben-Ari 2001; 2002; Ben-Ari et al. 2007; Ben-Ari 2012). In addition, both intrinsic properties of neurons and synaptic transmission undergo dramatic changes during early postnatal development in a brain-area specific manner (Kriegstein et al. 1987; McCormick and Prince 1987; Burgard and Hablitz 1993; Ramoa and McCormick 1994; Bahrey and Moody 2003). Most studies on these developmental changes of the GABAergic system in the cortex have focused on the primary somatosensory cortex, visual cortex and hippocampus (Bartolini et al. 2013; Le Magueresse and Monyer 2013; Hensch 2016).

The barrel cortex (BC) is part of the primary somatosensory cortex and is organized vertically in columns of cells associated with sensory perception (Guo et al. 2014) and horizontally in six layers of distinct cell types. In contrast, cortical association areas such as the prefrontal cortex (PFC) regulate cognitive functions and do not directly control sensory information (Fuster 2015). Anatomically, the mouse medial PFC (mPFC) is defined as the agranular part of frontal lobe, lacking the prominent granular layer IV and is divided into distinct subregions, namely infralimbic, prelimbic and cingulate cortex (Heidbreder and Groenewegen 2003; Van De Werd et al. 2010). The timeline of mPFC development is delayed compared to other sensory cortices, such as BC (Casey et al. 2000; Best and Miller 2010; Kolb et al. 2012, Rinetti-Vargas et al., 2017). From infancy to adulthood, the developing mPFC undergoes considerable transcriptional, structural and functional changes (Diamond 2005; Tsujimoto 2008; Kolb et al. 2012; Schubert et al. 2014; Kroeze et al. 2017).

While adolescent development of prefrontal circuitry and the underlying cellular mechanisms have been addressed by a large number of studies, few investigations tackled the wiring processes at earlier stages (Brockmann et al. 2011; Bitzenhofer et al. 2015; 2017), in particular the mPFC between the second (neonatal) and third (juvenile) postnatal week. Here, we aim to fill this gap by investigating the synaptic and intrinsic properties of neonatal and juvenile mPFC neurons, with a primary focus on the GABAergic system, and identifying their contribution to the development of network activity.

Methods

All *in vitro* experiments with mice took place under an experimental protocol approved by the Research Ethics Committee and by our Institutional Animal Care and Use Committee that has been approved by the Veterinarian Authorities Office (protocol license no. 93164). Experiments were carried out by trained scientists and in accordance with the 3R principles. *In vivo* experiments were performed in compliance with the German laws and the guidelines of the European Community for the use of animals in research and were approved by the local ethical committee (015/17, 015/18).

Animals

The *in vitro* experiments were performed on male C57Bl/6J; Lhx6Tg(Cre); R26R-YFP+/+ mice from animal facility of IMBB-FORTH were used. For the *in vivo* experiments, timed-pregnant

96 C57BL/6J mice from the animal facility of the University Medical Center Hamburg-Eppendorf
97 were used. The day of vaginal plug detection was defined as embryonic day (E)0.5, whereas the
98 day of birth was defined as P0. The offspring of both sexes are used for *in vivo* electrophysiology
99 recordings. All procedures were performed according to the European Union ethical standards
100 outlined in the Council Directive 2010/63EU of the European Parliament on the protection of
101 animals used for scientific purposes.
102 Mice were housed with their mothers and provided with standard mouse chow and water ad
103 libitum, under a 12 h light/dark cycle (light on at 7:00 am) with controlled temperature (21°C).
104 The P10 experimental group includes ages P9-P11 and the P20 group includes ages P19-P21, also
105 referred to as second and third postnatal weeks or neonatal and juvenile, respectively. All efforts
106 were made to minimize both the suffering and the number of animals used.
107
108 ***In vitro* extracellular recordings**
109 Slice Preparation*:* Mice (P10 and P20) were decapitated under halothane anesthesia. The brain
110 was removed promptly and placed in ice cold, oxygenated (95% O_2 –5% CO_2) artificial
111 cerebrospinal fluid (aCSF) containing (in mM): 125 NaCl, 3.5 KCl, 26 $NaHCO_3$, 1 $MgCl_2$ and 10
112 glucose (pH = 7.4, 315 mOsm/l). The brain was blocked and glued onto the stage of a vibratome
113 (Leica, VT1000S). Rostrocaudal coronal slices (400 µm thick) containing either the mPFC
114 (prefrontal cortex) or the BC (barrel cortex) region were selected and transferred to a submerged
115 chamber, which was continuously superfused with oxygenated (95% O_2 –5% CO_2) aCSF
116 containing (in mM): 125 NaCl, 3.5 KCl, 26 $NaHCO_3$, 2 $CaCl_2$, 1 $MgCl_2$ and 10 glucose (pH = 7.4, 315
117 mOsm/l) at room temperature (RT). The slices were allowed to equilibrate for at least 1 h in this
118 chamber before recordings began. Slices were then transferred to a submerged recording
119 chamber, continuously superfused with oxygenated (95% O_2 –5% CO_2) aCSF (same constitution
120 as the one used for maintenance of brain slices) at RT during recordings.
121 Data Acquisition: Electrophysiological recordings were performed in all experimental groups
122 under the same conditions as described below. Pulled glass micropipettes were filled with NaCl
123 (2M) and placed in layers II/III of PFC and BC. Platinum/iridium metal microelectrodes (Harvard
124 apparatus United Kingdom, 161 Cambridge, United Kingdom) were placed on layer II/III of the
125 mPFC and the BC, about 300 µm away from the 1MΩ recording electrode, and were used to
126 evoke field excitatory postsynaptic potentials (fEPSPs). Local field potentials (LFPs) were
127 amplified using a headstage with selectable high pass filter of 30 Hz to remove any offsets

128 coupled to a Dagan BVC-700A amplifier, amplified 100 times and low-pass filtered at 1-kHz. A
129 notch filter was used to eliminate line frequency noise at 30 Hz. Signals were digitized using the
130 ITC-18 board (InstruTech, Inc.) on a PC with custom-made procedures in IgorPro (Wavemetrics,
131 Inc.) and stored on a PC hard drive. All voltage signals were collected at a sampling frequency of
132 100 kHz (fs = 100 kHz).
133 For evoked fEPSPs, the electrical stimulus consisted of a single square waveform of 100 μs
134 duration given at intensities of 0.1– 0.3 mA (current was increased from 0.1 mA to 0.3 mA, with
135 0.1 mA steps) generated by a stimulator equipped with a stimulus isolation unit (World Precision
136 Instruments, Inc.). The effect of $GABA_AR$ activation was investigated by bath application of 2 μM
137 Diazepam ($GABA_AR$ agonist). Diazepam was acquired from the Pharmacy of the University
138 General Hospital in Heraklion as a 5 mg/ml solution and was diluted in aCSF during recordings.
139 Other drugs used include CNQX (10μM), AP5 (50μM) and bumetanide (10μM) (Tocris). For
140 spontaneous activity recordings, 20 5-sec recordings were acquired without any stimulation.
141 Data Analysis: Data were analyzed using custom-written procedures in IgorPro software
142 (Wavemetrics, Inc.). No additional high-pass filters were applied to the raw data. For evoked
143 recordings, the peak values of the fEPSP were measured using the minimum value of the synaptic
144 response (4–5 ms following stimulation) and were compared to the baseline value prior to
145 stimulation. Both parameters were monitored in real- time in every experiment. A stimulus–
146 response curve was then plotted using stimulation intensities between 0.1 and 0.8 mA, in 0.1
147 mA steps. For each different intensity level, two traces were acquired and averaged.
148
149 ***In vitro* patch-clamp recordings**
150 Slice Preparation: Mice were decapitated under halothane anesthesia. The brain was removed
151 immediately and coronal slices of mPFC and BC (300–350 μm thick), using a vibratome (Leica,
152 VT1000S, Leica Biosystems) were prepared from mice at the ages of P10 and P20 in ice-cold
153 oxygenated (95% O_2 - 5% CO_2) modified choline-based aCSF (in mM) 0.5 $CaCl_2$, 7 mM $MgSO_4$;
154 NaCl replaced by an equimolar concentration of choline). Slices were incubated for 30min at
155 32^oC in an oxygenated normal aCSF containing (in mM): 126 NaCl, 3.5 KCl, 1.2 NaH_2PO_4, 26
156 $NaHCO_3$, 1.3 $MgCl_2$, 2.0 $CaCl_2$, and 10 D-glucose, pH 7.4, 315 mOsm/l. Slices were allowed to
157 equilibrate for at least 30 min at RT before being transferred to the recording chamber. During
158 recordings, slices were perfused at a rate of 4 ml/min with continuously aerated (95% O_2-5%
159 CO_2) normal aCSF at RT.

Data Acquisition: Neurons were impaled with patch pipettes (5–7 MΩ) and recorded in the whole-cell configuration, either in the current-clamp or voltage-clamp mode. For current-clamp experiments, the composition of the intracellular solution was: 130 mM K-$MeSO_4$, 5 mM KCl, 5 mM NaCl, 10 mM HEPES, 2.5 mM Mg-ATP, and 0.3 mM GTP, 265–275 mOsm, pH 7.3. To measure neuronal excitability and passive membrane properties a 500ms step-pulse protocol was used with current stimulation from -200pA to +50pA. To measure action potential properties, a 5ms step-pulse protocol was used.

For voltage-clamp experiments, the composition of the intracellular solution was: 120 mM Cs-gluconate, 20mM CsCl, 0.1 mM $CaCl_2$, 1 mM EGTA, 0.4 mM Na-guanosine triphosphate, 2mM Mg-adenosine triphosphate, 10 mM HEPES. For perforated patch-clamp recordings, patch pipettes were front-filled with the above intracellular solution and back-filled with the same solution containing 5µg/ml gramicidin. No correction from liquid junction potential was applied between the pipette and the aCSF. Whole-cell measurements were low-pass filtered at 5 kHz using an Axopatch 200B amplifier (Molecular Devices, Inc). Recordings were digitized with the ITC-18 board (Instrutech, Inc) on a PC using custom-made codes in IgorPro (Wavemetrics, Inc). All signals were collected at a sampling frequency of 20kHz. For voltage-clamp recordings, the composition of the intracellular solution was:

Data Analysis: Data were analyzed using custom-written codes in IgorPro software (Wavemetrics, Inc.). For passive membrane properties, the resting membrane potential (RMP, mV) was measured within 3 min after establishing the whole-cell configuration, and monitored throughout the experiment. To measure input resistance, a 500ms step-pulse protocol was used with current stimulation from -200pA to +50pA. The input resistance (R_{in}, MΩ) was measured by plotting the steady-state voltage deflection in an I-V plot and calculating the slope of the best fit line curve (R_{in}=V/I). The τ_m (membrane time constant, ms) was obtained by fitting a single exponential curve to the voltage deflection at -50pA, and the membrane capacitance (C_m) was calculated using the formula $C_m = \tau_m/R_{in}$. In addition, the number of spikes generated in response to a 500ms step-pulse range from +100pA to +300pA was measured.

To measure action potentials (APs) properties, we applied small supra-threshold 5ms step-pulse currents to the cell from -65mV. The active properties were measured at the minimum current stimulation (Rheobase, pA) that generated an AP. The AP threshold (mV) was calculated by taking the first derivative of the voltage trace, defining a threshold and identifying the voltage

192 level at that time point. The rate of rise of the AP (dV/dt, mV/ms) was the maximum value of
193 that first derivative trace. The AP amplitude (mV) was defined as the voltage difference between
194 AP threshold and AP peak. The AP duration (ms) was calculated by the full width of the waveform
195 at the half maximal amplitude (half-width). The fast afterhyperpolarization (fAHP) minimum
196 (mV) was defined as the minimum voltage value right after the AP. The fAHP amplitude (mV)
197 was calculated as the difference between the AHP minimum and the AP threshold. The fAHP
198 time (ms) was defined as the time duration from the time point of AP threshold to the fAHP
199 minimum.
200
201 The measurements of spontaneous excitatory postsynaptic currents (sEPSCs) were taken at -
202 60mV and for spontaneous inhibitory postsynaptic currents (sIPSCs) at +10mV. Automatically
203 selected events were subsequently visually monitored to discard erroneously included noise.
204 The events showing only single peaks were selected for kinetics analysis. All currents detected
205 from every single neuron were averaged. The peak amplitude was calculated as the maximum
206 current value. The time constant of the decay phase was detected by curve fitting with a single
207 exponential decay function.
208 To investigate the IPSC reversal potential, a stimulating electrode was positioned 100µm away
209 from the recording electrode at the border between layer I and layer II. Recordings were taken
210 at different voltage steps, from -80mV to +40mV in the presence of CNQX (20µM) and AP5
211 (50µM).
212
213 **Immunohistochemistry**
214 Mice at the age of P10 and P20 were perfused with 4% paraformaldehyde, followed by fixation
215 with the same solution for 1h at 4◦C, followed by cryoprotection and preparation of 12 µm
216 cryostat sections as previously described (Vidaki et al., 2012). Primary antibodies used were rat
217 monoclonal anti-GFP (Nacalai Tesque, Kyoto, Japan, 1:5000), rabbit polyclonal anti-GFP (1:500;
218 Minotech Biotechnology, Heraklion, Greece) and rabbit polyclonal anti-parvalbumin (PV)
219 (Swant, Bellinzona, Switzerland; 1:2000. Secondary antibodies used were goat anti-rat-Alexa
220 Fluor-488, goat anti-rabbit Alexa Fluor-488, and goat anti-rabbit-Alexa Fluor-555 (Molecular
221 Probes, Eugene, OR, United States, 1:800). Images were obtained with a confocal microscope
222 (Leica TCS SP2, Leica, Nussloch, Germany). For each age group (P10, P20), 2-4 10µm-thick
223 sections from each mouse brain were selected, all including the mPFC and BC.

224

225 **RNA *In Situ* Hybridization**

226 Non-radioactive *in situ* hybridization experiments were performed on cryostat sections (12µm
227 thick, see immunochemistry) according to the protocol described (Schaeren-Wiemers and
228 Gerfin-Moser 1993). Riboprobe was prepared by *in vitro* transcription and was specific
229 Somatostatin (SST) (Liodis et al. 2007).

230

231 **Nissl Staining**

232 Cryostat sections (12µm thick, see immunochemistry) were incubated in 1:1 100%
233 ethanol:chloroform overnight at RT. Then, sections were rehydrated for 1 min in 100%, 95%
234 ethanol solutions and dH_2O at RT, followed by a 10-min incubation in 0.1% cresyl violet solution
235 at 50°C. Sections were then dehydrated with dH_2O, 95%, 100% ethanol and xylene for 5 min and
236 coverslipped with permount. Images from whole sections were obtained in 5× magnification of
237 a light microscope (Axioskop 2FS, Carl Zeiss AG, 268 Oberkochen, Germany) and merged using
238 Adobe Photoshop CC 2015, Adobe Systems, Inc.

239

240 **Analysis for Immunochemistry, *in situ* hybridization and Nissl staining**

241 Images taken from Nissl staining slices were analyzed with Matlab, using a custom-made
242 algorithm, which was double checked with hand-counting (Konstantoudaki et al. 2016;
243 Chalkiadaki et, 2019). Images from immunochemistry and in situ hybridization experiments,
244 were hand counted using ImageJ.

245

246 **Western blots**

247 Mice were decapitated following cervical dislocation, the brain was quickly removed, placed in
248 ice cold PBS (phosphate-buffered saline) and then positioned on a brain mold, where 1.5 mm
249 slices were taken containing the mPFC and BC. The slices were placed on dry ice, and the
250 prelimbic area of mPFC was dissected out and stored at -80°C. The BC was also isolated from the
251 corresponding slices and stored at -80°C. Frozen tissue blocks were lysed in a solution containing
252 (in mM) HEPES 50, NaCl 150, MgCl2 1.5, EGTA 5, Glycerol 1%, Triton-X100 1%, 1:1000 protease
253 inhibitors cocktail. Proteins ran on 8.5% bis-acrylamide gel and were transferred onto a
254 nitrocellulose membrane (Whatman GmbH, Dassel, Germany). The membrane was blocked,
255 incubated in rabbit polyclonal anti-K+/Cl-Cotransporter (KCC2) (Merck KGaA, Darmstadt,

256 Germany, 1:1000) or rabbit monoclonal anti-GAPDH (Cell Signaling Technology Europe BV,
257 Leiden, Netherlands, 1:1000), washed, incubated in secondary goat anti-rabbit IgG Horseradish
258 Peroxidase Conjugate antibody (Invitrogen, 1:5000), and digitally exposed using the Molecular
259 Imaging system ChemiDoc (BioRad Laboratories, Inc, California, U.S.A.). Analysis of KCC2 and
260 GAPDH expression was performed with ImageJ software, and the raw values of KCC2 from each
261 sample were normalized to their respective GAPDH values.
262
263 **Statistical analysis**
264 Statistical analyses were performed in Microsoft Office Excel 2007 and GraphPad Prism Software
265 7.0. Data are presented as mean ± standard error of mean (SEM). Normality distribution and
266 equality of variances of dataset were tested with the Kolmogorov-Smirnov test normality test.
267 The null hypothesis was rejected for a >5%. When four experimental groups (P10 mPFC, P20
268 mPFC, P10 BC and P20 BC) were assessed and two variables were taken into consideration (age
269 and brain area), data were analyzed with a two-way ANOVA with Fisher LSD, Sidak's or Tukey's
270 multiple comparisons (electrophysiological recordings and cell counting). When three groups
271 (P10 mPFC, P20 mPFC and P10 BC) data were analyzed with one-way ANOVA
272 (electrophysiological recordings). Significant differences were detected by one-way ANOVA.
273 Significance levels of *$p < 0.05$, **$p < 0.01$, ***$p < 0.001$ or ****$p < 0.0001$ were tested. For
274 comparison of Western blot analysis, the significant effect of each developmental age group
275 from mPFC and BC was assessed using Student's t-test depending on the experiment.
276
277 **Modeling**
278 We adapted the PFC microcircuit model we had developed previously (Konstantoudaki et al.,
279 2014) to fit our experimental data with regards to intrinsic properties of pyramidal neurons and
280 fast-spiking interneurons. We generated two model networks: a) a neonatal mPFC model
281 network and b) a juvenile mPFC model network. In the neonatal mPFC model network the
282 following adjustments were made: a) the pyramidal model neuron was adjusted to fit the passive
283 and active properties of the neurons recorded in this paper, primarily the neonatal pyramidal
284 model neuron exhibited increased input resistance and reduced spike amplitude, b) the fast-
285 spiking interneuron model neuron was adjusted to have reduced fast afterhyperpolarization, as
286 found in our experiments and c) the $GABA_AR$ receptor model had a reversal potential of -40mV.
287 In the juvenile mPFC model network, the following adjustments were made: a) the $GABA_AR$

288 receptor model had a reversal potential of -60mV. All other properties were maintained as in
289 the original model. The network was stimulated with spontaneous synaptic activation on
290 pyramidal model neurons with characteristics similar to the sEPSC and sIPSC properties we
291 recorded. Each condition was simulated in 10 different trials. In each trial, the location of
292 activated synapses varied.
293
294 **Data availability**
295 Data presented in the figures in this paper are available upon request. The model networks will
296 be uploaded on ModelDB once published.
297
298 **Results**
299 Mice belonging to two age groups were investigated: (i) neonatal mice included pups of
300 postnatal days (P) 9-11 and are defined as P10 while (ii) juvenile mice defined as P20 animals
301 included pups of P19-P21. Due to the high density of intra-cortical synapses in the superficial
302 cortical layers (DeFelipe and Fariñas 1992; Clancy et al. 2001) and their specific involvement in
303 neurodevelopmental disorders (Chini and Hanganu-Opatz, 2020; Bitzenhofer eta l., 2017), we
304 focused on the superficial layers of the mPFC and BC. All analyses that had four groups (mPFC
305 P10 and P20, BC P10 and P20) were conducted using two-way ANOVA, with the two factors being
306 the brain area (mPFC and BC) and age (P10 and P20).
307
308 **Synaptic transmission adaptations in mPFC and BC across development**
309 To examine spontaneous synaptic transmission, we performed patch-clamp recordings from
310 layer II/III pyramidal neurons in mPFC and BC from neonatal and juvenile mice. We recorded
311 spontaneous inhibitory postsynaptic currents (sIPSCs, at +10mV) and spontaneous excitatory
312 postsynaptic currents (sEPSCs, at -60mV) and we measured the frequency, amplitude and decay
313 time constant.
314 In mPFC, the frequency of sIPSCs was significantly augmented in the juvenile group compared to
315 the neonatal group (**Figure 1a,b**), while the sIPSC amplitude and decay-time constant did not
316 significantly change over the investigated time window (**Figure 1a,c,d**). Similarly, the sIPSC
317 frequency and amplitude were significantly increased, in the juvenile compared to the neonatal
318 BC (**Figure 1a,b,c**), while the decay-time constant was not altered (**Figure 1a,d**). On a different

319 note, the sIPSC frequency in BC in the juvenile group was significantly increased compared to the
320 neonatal group in BC but also compared to the juvenile group in mPFC.
321 The sEPSC frequency was significantly decreased in the juvenile compared to the neonatal group,
322 in both areas (**Figure 1e,f**), while the amplitude and decay time constant were unaltered (**Figure**
323 **1g,h**). Upon comparing the two brain areas, the sEPSC frequency and amplitude were found
324 significantly decreased in mPFC, compared to BC, in the neonates (**Figure 1f**). In juvenile mice,
325 the sEPSC frequency was similar between the two cortical areas, while the amplitude remained
326 significantly smaller in mPFC compared to BC in both ages (**Figure 1g**). The decay time constant
327 was not different between areas at both ages (**Figure 1h**).
328 We further investigated the changes in sIPSC and sEPSC frequency changes in the mPFC, in
329 particular, in the presence of AMPA and NMDA receptor antagonists, CNQX and AP5, respectively
330 and a $GABA_A$ receptor antagonist, bicuculine. The sIPSC frequency remained increased in the
331 juvenile group, compared to the neonatal group, CNQX and AP5 (**Figure 2a,c**). On the other hand,
332 bicuculine blocked the sIPSCs both in the mPFC at both ages (**Figure 2 b, c**). Application of CNQX
333 eliminated the sEPSCs in juvenile mPFC slices and significantly reduced, but did not eliminate
334 sEPSCs, in neonatal mPFC slices (**Figure 2e,g**). Application of bicuculine (10uM) did not affect the
335 sEPSC frequency in juvenile mPFC slices but significantly reduced sEPSC frequency in the neonatal
336 mPFC (**Figure 2f,g**). These results suggest that depolarizing $GABA_AR$ currents could contribute to
337 the increased sEPSC frequency observed in layer II/III mPFC pyramidal neurons in the neonatal
338 group.
339
340
341

Figure 1

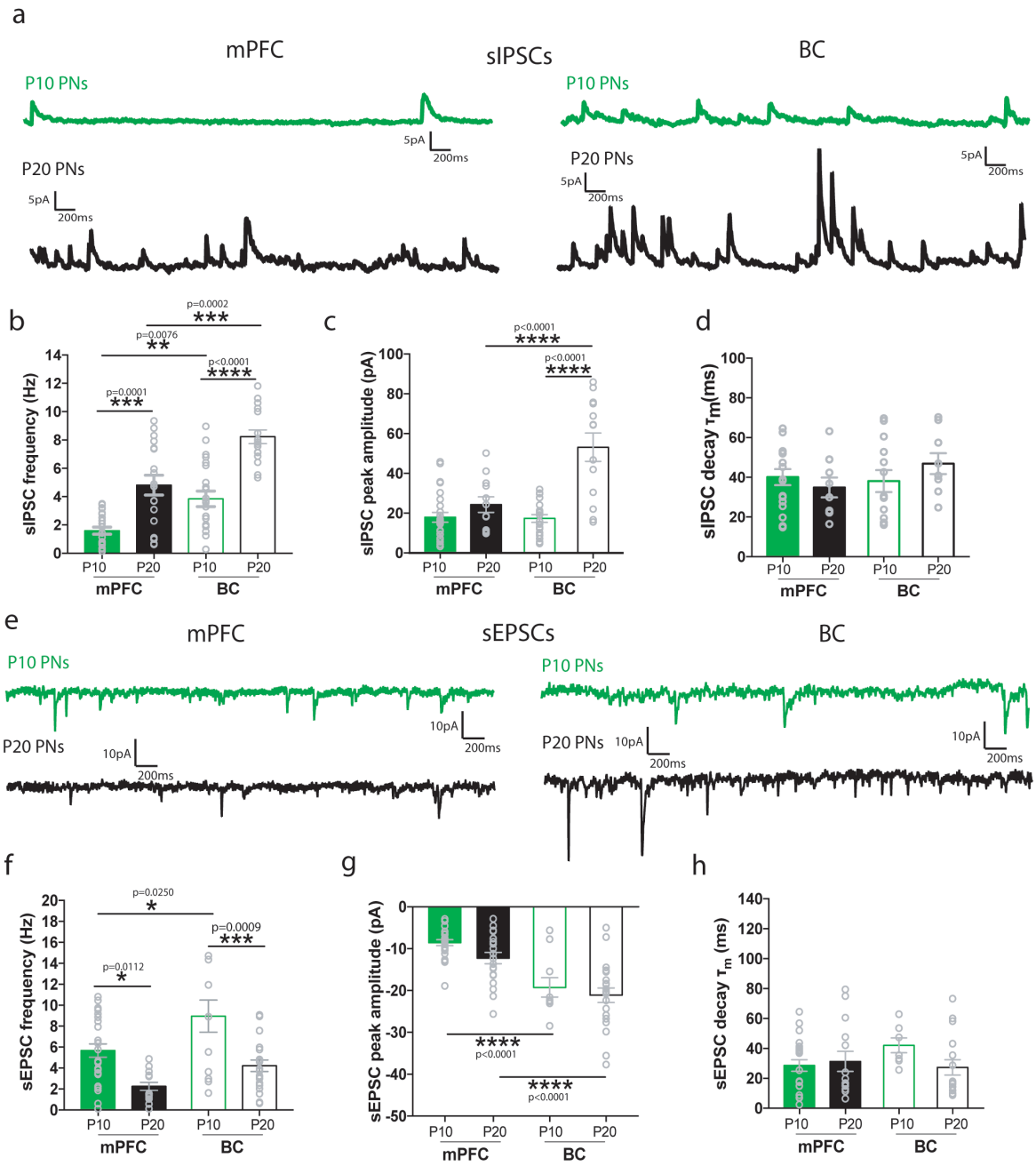

Figure 1. Properties of sIPSCs and sEPSCs at P10 and P20 of layer II/III mPFC and BC pyramidal neurons

(a) *Representative traces of spontaneous inhibitory postsynaptic currents (sIPSCs) from layer II/III mPFC (left) and BC (right) pyramidal neurons at P10 (green) and P20 (black).*

(b) *Bar graph showing the sIPSC frequency (Hz) at P10 and P20 mPFC and BC pyramidal neurons. Two-way ANOVA analyses showed a significant effect of age ($F_{(1,26)}$=19.286, p<0.001) and brain area ($F_{(1,26)}$=12.554, p=0.002) and a trend towards significance of age*brain interaction ($F_{(1,26)}$=3.826, p=0.063).*

351 ***(c)*** *Bar graph showing the sIPSC peak amplitude at P10 and P20 of mPFC and BC pyramidal*
352 *neurons. Two-way ANOVA analyses showed a trend towards significance in the brain area factor*
353 *($F_{(1,26)}$=3.420, p=0.077) and no effect of age ($F_{(1,26)}$=1.981 p=0.177) or area*age interaction*
354 *($F_{(1,26)}$=0.050, p=0.826).*
355 ***(d)*** *Bar graph showing the sIPSC decay time constant (τm) at P10 to P20 of mPFC and BC*
356 *pyramidal neurons. Two-way ANOVA analyses did not show any significant effect of age*
357 *($F_{(1,26)}$=1.129, p=0.299), brain area ($F_{(1, 26)}$=0.211, p=0.651) or area*age interaction ($F_{(1, 26)}$=1.052,*
358 *p=0.316) was found.*
359 ***(e)*** *Representative traces of spontaneous excitatory postsynaptic currents (sEPSCs) from layer*
360 *II/III mPFC (left) and BC (right) pyramidal neurons at P10 (green) and P20 (black).*
361 ***(f)*** *Bar graph showing the sEPSC frequency at P10 to P20 of mPFC and BC pyramidal neurons.*
362 *Two-way ANOVA analyses showed a significant effect of age ($F_{(1,25)}$=5.273, p=0.032) and brain*
363 *area ($F_{(1,25)}$=7.388, p=0.013), but not a significant interaction age*brain area ($F_{(1,25)}$=0.591,*
364 *p=0.450)*
365 ***(g)*** *Bar graph showing the sEPSCs peak amplitude at P10 to P20 of mPFC and BC pyramidal*
366 *neurons. Two-way ANOVA analyses did not reveal significant effect of brain area ($F_{(1,25)}$=0.853,*
367 *p=0.366), age ($F_{(1,25)}$=0.144, p=0.708) or interaction ($F_{(1,25)}$=0.712, p=0.408).*
368 ***(h)*** *Bar graph showing the sEPSCs decay time constant (τm) at P10 to P20 of mPFC and BC*
369 *pyramidal neurons. Two-way ANOVA analyses showed no significant effect of age ($F_{(1,25)}$=0.557,*
370 *p=0.463), brain area ($F_{(1,25)}$=0.720, p=0.405) or interaction ($F_{(1,25)}$=1.128, p=0.300).*
371 **n=9-13 cells from 5-9 mice/age group.*
372

Figure 2

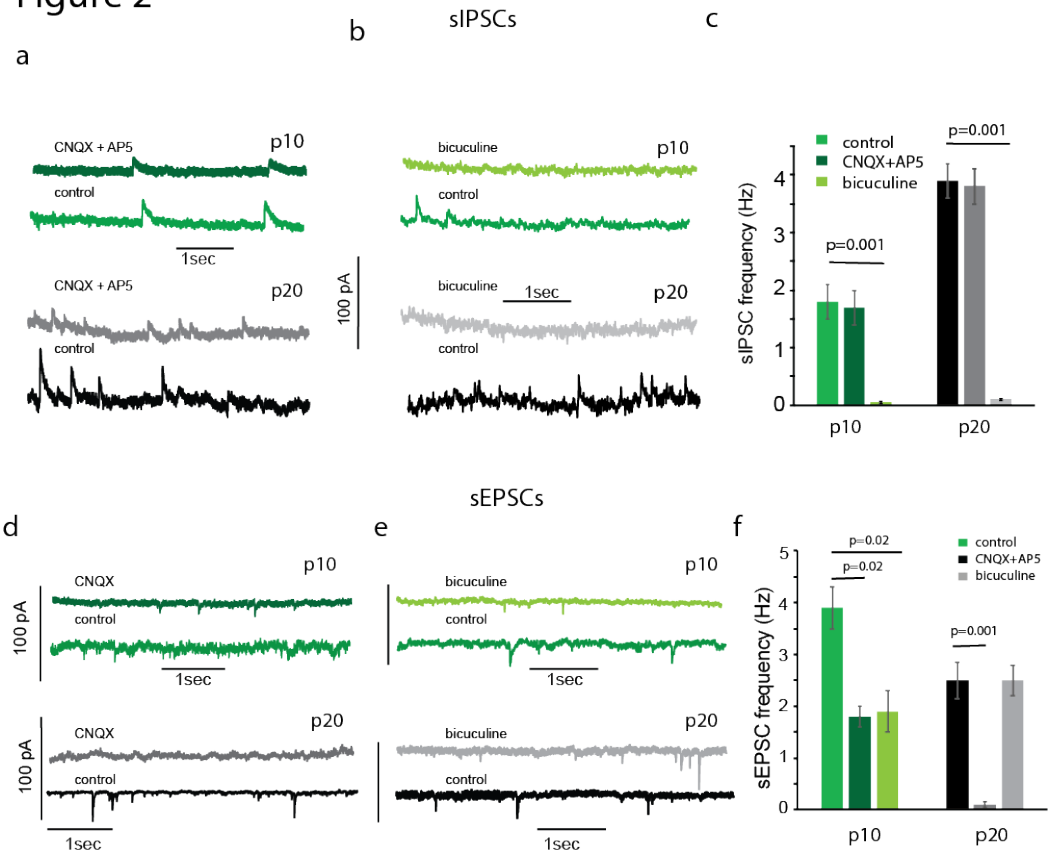

Figure 2- sIPSCs and sEPSCs frequency at P10 and P20 of layer II/III mPFC and BC pyramidal neurons

(a) *Representative traces showing that CNQX+AP5 did not alter the sIPSC frequency either at P10 or P20 mPFC (recorded at +10mV).*

(b) *Representative traces showing that bicuculine blocks sIPSCs either at P10 or P20 mPFC (recorded at +10mV).*

(c) *Graphs showing that bicuculine blocks the sIPSCs in P10 and P20 mPFC (t-test, p=0.001), while CNQX+AP5 does not have an effect (t-test, p=0.5).*

(d) *Representative traces showing that CNQX reduces sEPSC frequency at p10 and blocks sEPSCs at P20 mPFC (recorded at -70mV).*

(e) *Representative traces showing that bicuculine reduces sEPSC frequency at p10 and does not affect sEPSCs at P20 mPFC (recorded at -70mV).*

(f) *Graphs showing that at P10 mPFC both CNQX+AP5 and bicuculine reduces the sEPSC frequency in P10 mPFC (t-test, p=0.03 for both drugs), while in P20 mPFC only CNQX+AP5 blocks sEPSCs.*

390 **GABA is depolarizing in the neonatal mPFC but not BC**

391 Our data so far suggests that $GABA_AR$ function is still depolarizing in the mPFC in neonates. To
392 further investigate this, we performed perforated patch-clamp recordings and recorded evoked
393 IPSCs (eIPSCs) in the mPFC at both ages in the presence of CNQX and AP5 at different voltage
394 steps. A line curve was fit across the eIPSC currents recorded from -60mV to +10mV, because
395 there was a linear V-I relationship at this range. From the graphs, it is evident that reversal
396 potential at P10 is more positive than -30mV, while the reversal potential at P20 is around -45mV
397 (**Figure 3a,b**).

398

Figure 3

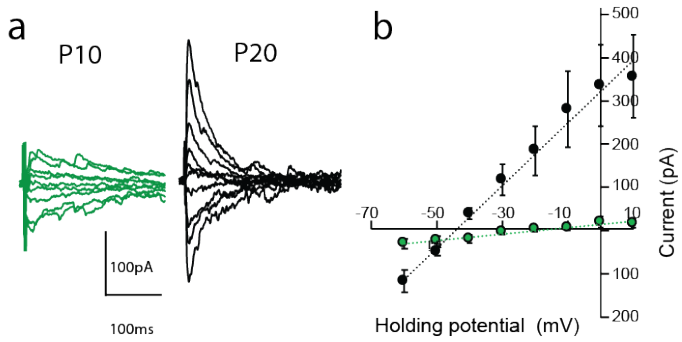

399

400 ***Figure 3 – The reversal potential for evoked IPSCs is depolarized at p10 mPFC compared to p20***

401 *(a) Representative traces of evoked IPSCs at p10 and p20 mPFC*

402 *(b) Graph showing the average of eIPSCs at different holding potentials.*

403

404 We further investigated the $GABA_AR$ activity by isolating a $GABA_AR$ response in fEPSP recordings
405 by using CNQX and AP5. The addition of diazepam (2µM) (a $GABA_AR$ agonist) increased the fEPSP
406 amplitude in mPFC in the neonatal but not juvenile groups (**Figure 4a-b**). In BC, there was no
407 effect of diazepam, at either age (**Supplemental Figure 1**). The switch in the $GABA_AR$ function
408 from depolarizing to hyperpolarizing occurs due to the increased expression of the K^+-Cl^- co-
409 transporter 2 (KCC2) (Rivera et al. 1999). To determine whether modulating chloride
410 transporters could alter the diazepam-induced enhancement of the fEPSP at P10 mPFC, we
411 recorded the fEPSP in the presence of bumetanide (10uM), which blocks the NKCC1 transporter,
412 and tested the effect of diazepam. We find that in the presence of bumetanide, diazepam did
413 not result in an increase of the fEPSP (**Figure 4c-d**). In addition, we demonstrated that KCC2
414 protein levels were significantly increased in the juvenile compared to the neonatal mPFC but

415 not in the BC (**Figure 4e-g**). The above results collectively suggest that the $GABA_AR$ function is
416 depolarizing in the neonatal mPFC.

Figure 4

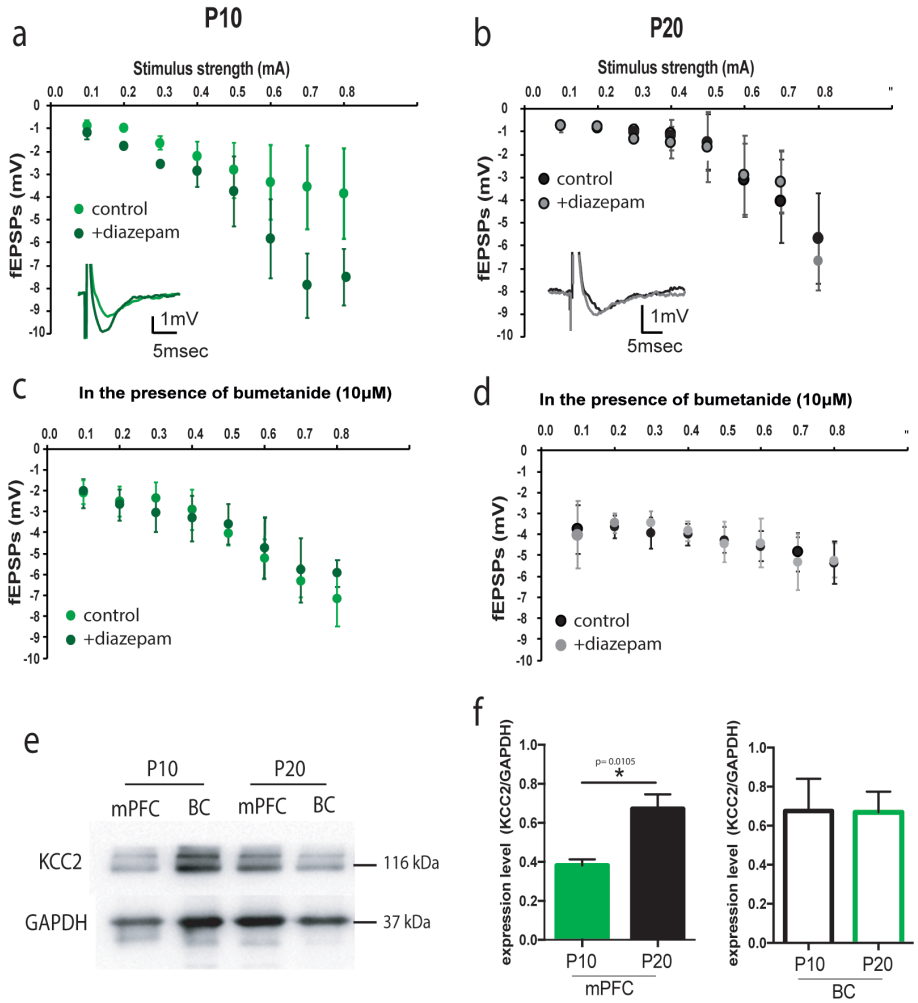

417

418 ***Figure 4. Changes in the chloride transporters mediate the depolarizing action of $GABA_AR$ at***
419 ***P10 mPFC***

420 *fEPSPs were recorded were recorded in layer II/III mPFC in response to current pulses of*
421 *increasing stimulus strength of layer II/III, during two experimental treatments, before and after*
422 *application of 2μM diazepam ($GABA_AR$ agonist) at P10 and P20.*

423 ***(a)*** *Representative traces (left) and graph (right) showing the fEPSPs amplitude before (green)*
424 *and after (dark green) diazepam bath application (in the presence of CNQX and AP5), in mPFC at*
425 *P10. Two-way repeated measures ANOVA analyses of evoked fEPSPs revealed significant effect*
426 *of stimulus strength ($F_{(1,7)} = 20.64$, $p=0.004$) and experimental treatments ($F_{(1,7)} = 5.025$, $p=0.036$)*
427 *(n=2 brain slices from 3-4 mice).*

428 ***(b)*** *Graph (right) and representative traces (left) showing that diazepam bath application does*
429 *not have any effect on the fEPSP amplitude in mPFC at P20 (in the presence of CNQX and AP5).*
430 *Two-way repeated measures ANOVA analyses of evoked fEPSPs revealed a significant effect of*
431 *stimulus strength ($F_{(1,7)}$ = 10.36, p<0.0001) but not experimental treatment ($F_{(1,7)}$=0.03,*
432 *p=0.9382), (n=2 brain slices from 3-4 mice).*
433 ***(c)*** *Graph showing that the effect of diazepam on fEPSP is occluded in the presence of*
434 *bumetanide (plus CNQX and AP5) at P10. Two-way repeated measures ANOVA analyses of*
435 *evoked fEPSPs did not reveal a significant effect of experimental treatment ($F_{(1,7)}$=0.08, p=0.752),*
436 *(n=2 brain slices from 3-4 mice).*
437 ***(d)*** *Graph showing the effect of diazepam on fEPSP in the presence of bumetanide (plus CNQX*
438 *and AP5) at P20. Two-way repeated measures ANOVA analyses of evoked fEPSPs did not reveal*
439 *a significant effect of experimental treatment ($F_{(1,7)}$=0.06, p=0.831), (n=2 brain slices from 3-4*
440 *mice).*
441 ***(e)*** *Representative blots showing changes of the K-Cl co-transporter (KCC2) levels, relative to*
442 *GAPDH at P10 and P20 in mPFC and BC.*
443 *(f) Graph showing the normalized protein level (KCC2/GAPDH) in mPFC at P10 and P20. The KCC2*
444 *protein levels was significantly increased at P20 compared to P10 in mPFC (two-tailed t-test, p=*
445 *0.01) but not in BC (two-tailed t-test, p= 0.97) (n=3-4 mice).*
446
447
448 **Passive and active membrane properties of MGE-derived interneurons are altered in the mPFC**
449 **across development**
450 To investigate whether additional changes in interneuron properties are present between
451 neonatal and juvenile groups, we performed current-clamp recordings from layer II/III mPFC and
452 BC of Lhx6^{+} interneurons. For this reason, Lhx6-cre;ROSA26fl-STOP-fl-YFP mice were used in
453 which Lhx6^{+} interneurons express YFP. Lhx6 is expressed by all post-mitotic and mature MGE-
454 derived interneurons (Liodis et al. 2007), therefore, YFP is expressed in MGE-derived
455 interneurons, which include interneurons that express parvalbumin (PV^{+}) and somatostatin
456 (SST^{+}).
457 Upon analysis of the passive properties, we found a significant increase in the input resistance
458 and membrane time constant, as well as a significant decrease in the membrane capacitance in
459 the neonatal compared to the juvenile mPFC (**Figure 5**). In addition, the input resistance and the

membrane time constant were higher in the neonatal mPFC, compared to BC (at both ages). There was no difference in the resting membrane potential (RMP) between ages and brain areas (**Figure 5, Supplementary Table 1**).

Regarding the active properties, there was no significant difference between ages and brain areas in the AP amplitude, AP threshold and rheobase, fAHP time (duration) (**Figure 5a, d, e, g; Supplementary Table 1**). The AP rate of rise (dv/dt) was significantly increased while the AP duration (half-width) was significantly reduced in the juvenile compared to the neonatal mPFC and BC (**Figure 6b,c, Supplementary Table 1**). In addition, the fAHP amplitude was significantly lower in the mPFC (**Figure 6f, Supplementary Table 1**), compared to BC. The increased rate of rise and the decreased AP duration are possibly linked with the up-regulation of voltage-dependent sodium channels during development (Huguenard et al. 1988), and in combination with the reduced fAHP amplitude suggest that the MGE-interneurons in neonatal mPFC are still quite immature, when compared to adult PV^+/SST^+ interneurons in the same region (Yang et al. 2013; Pan et al. 2017).

Overall, our data indicate that some intrinsic properties of interneurons in mPFC change with age (from P10 to P20), reaching values that closer resemble adult MGE-derived interneurons (Yang et al. 2013; Pan et al. 2017). The increased sIPSC frequency of mPFC pyramidal neurons observed in the juvenile group could partly be explained by these altered properties of presynaptic interneurons.

Figure 5

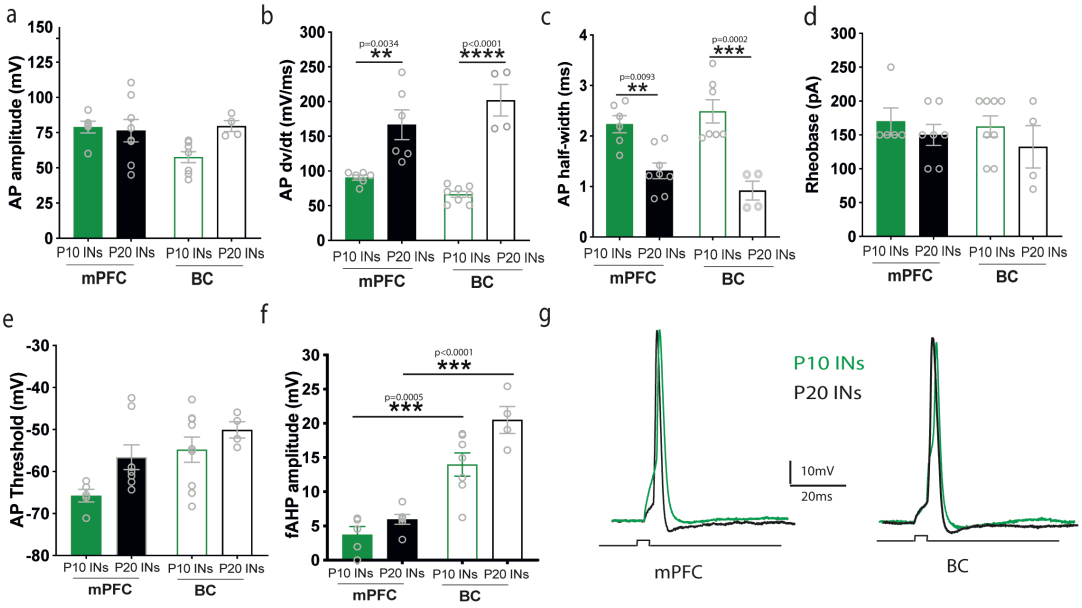

Figure 5. Poor development of active membrane properties of Lhx6⁺ interneurons in mPFC.

481 ***(a)*** *Bar graph showing the action potential (AP) amplitude of interneurons at P10 and P20 in*
482 *mPFC and BC. Two-way ANOVA analyses did not show any significant effect of age ($F_{(1,22)}$=2.46,*
483 *p=0.13) or brain area ($F_{(1, 22)}$=2.13, p=0.15) was found., (n=6-9 cells from 5-6 mice/age group).*
484 ***(b)*** *Bar graph showing the AP rate of rise (dv/dt) of interneurons at P10 and P20 in mPFC and at*
485 *P10 in BC. Two-way ANOVA analyses showed a significant effect between ages ($F_{(1,20)}$=58.96,*
486 *p<0.0001) but not brain area ($F_{(1,20)}$=0.16 p=0.69). Post-hoc analysis showed that the AP rate of*
487 *rise significantly increased at P20 compared to P10 in mPFC (Tukey's test, p=0.0034) and at P20*
488 *compared to P10 in BC (Tukey's test, p<0.001), (n=6-9 cells from 5-6 mice/age group).*
489 ***(c)*** *Bar graph showing the AP duration (half-width) of interneurons at P10 and P20 in mPFC and*
490 *BC. Two-way ANOVA analyses showed a significant effect between ages ($F_{(1,21)}$=39.16, p<0.0001)*
491 *but not brain area ($F_{(1,21)}$=0.16 p=0.73). Post-hoc analysis showed that the AP duration*
492 *significantly decreased at P20 compared to P10 in mPFC (Tukey's test, p= 0.0093) and at P20*
493 *compared to P10 in BC (Tukey's test, p=0.0002), (n=6-9 cells from 5-6 mice/age group).*
494 ***(d)*** *Bar graph showing the AP rheobase of interneurons at P10 and P20 in mPFC and BC. Two-*
495 *way ANOVA analyses did not show any significant effect of age ($F_{(1,20)}$=1.60, p=0.22) or brain area*
496 *($F_{(1, 20)}$=0.40, p=0.53) was found.*
497 ***(e)*** *Bar graph showing the AP threshold of interneurons at P10 and P20 in mPFC and BC. Two-*
498 *way ANOVA analyses showed significant effect of age ($F_{(1,22)}$=5.048, p=0.035) and brain area ($F_{(1,}$*
499 *$_{22)}$=8.00, p=0.009) was found. Post-hoc analysis showed that the AP threshold was not*
500 *significantly different at P20 compared to P10 in mPFC (Tukey's test, p=0.1673) and in BC (Tukey's*
501 *test, p=0.72009) or at P10 in mPFC compared to P10 in BC (Tukey's test, p=0.067) and at P20 in*
502 *mPFC compared to P20 in BC (Tukey's test, p=0.72).*
503 ***(f)*** *Bar graph showing the AHP (afterhypolarization) amplitude of interneurons at P10 and P20*
504 *in mPFC and BC. Two-way ANOVA analyses showed significant effect of age ($F_{(1,18)}$=7.35,*
505 *p=0.0143) and brain area ($F_{(1, 18)}$=63.72, p<0.0001) was found. Post-hoc analysis showed that the*
506 *AHP amplitude was not significantly different at P20 compared to P10 in mPFC (Tukey's test,*
507 *p=0.7187) and was significantly decreased in mPFC compered to BC, at P10 (Tukey's test, p=*
508 *0.0005) and in mPFC compered to BC at P20 (Tukey's test, p<0.00001), (n=6-9 cells from 5-6*
509 *mice/age group).*
510 ***(g)*** *Bar graph showing the AHP time of interneurons at P10 and P20 in mPFC and BC. Two-way*
511 *ANOVA analyses did not show any significant effect of age ($F_{(1,19)}$=0.009, p=0.92) or brain area*
512 *($F_{(1, 19)}$=1.074, p=0.31) was found.*

513 ***(h)*** *Representative traces of APs of layer II/III Lhx6+ interneurons in mPFC (left) and BC (right) at*
514 *P10 (green) and P20 (black).*
515

Figure 6

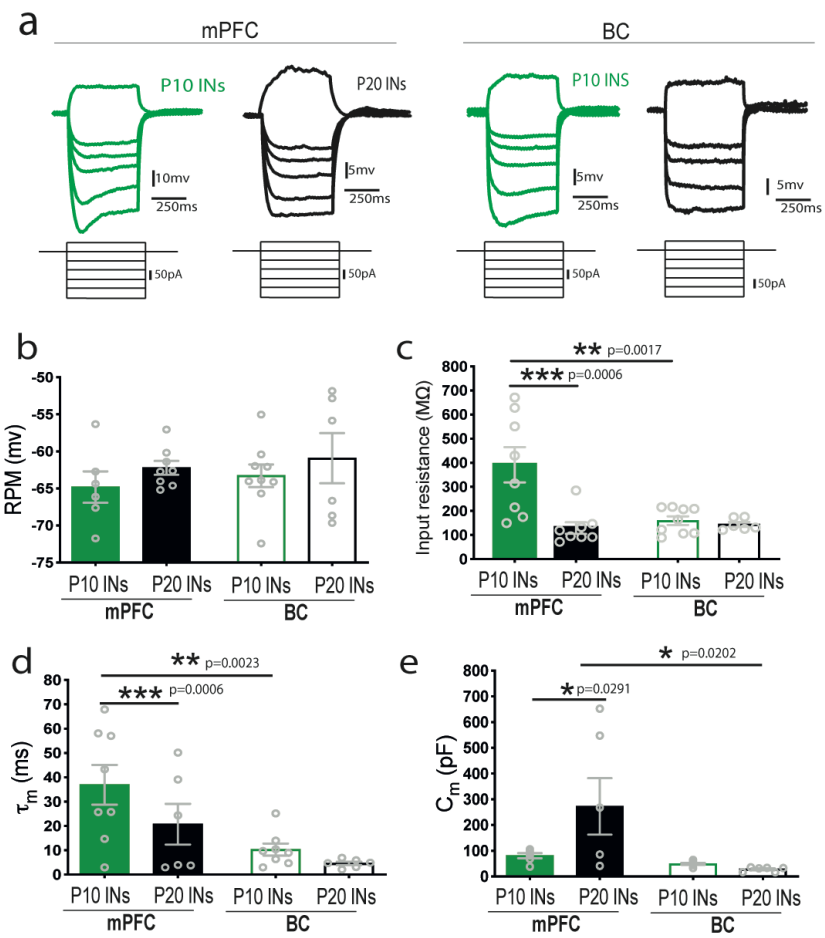

516
517 ***Figure 6. Passive membrane properties of Lhx6+ interneurons at P10 and P20 mPFC and P10***
518 ***BC.***
519 ***(a)*** *Representative voltage responses (top traces) to 500ms positive and negative current pulses*
520 *(bottom traces, +50, -50, -70, -100, -150, -200 pA) in mPFC at P10 and P20 and BC of Lhx6+*
521 *florescent interneurons from layer II/III.*
522 ***(b)*** *Bar graph showing the resting membrane potential (RMP) of interneurons at P10 and P20 in*
523 *mPFC and BC. Two-way ANOVA analyses did not show any significant effect of age ($F_{(1,25)}$=1.55,*
524 *p=0.22) or brain area ($F_{(1, 25)}$=0.50, p=0.48) was found., (n=6-9 cells from 5-6 mice/age group).*
525 ***(c)*** *Bar graph showing the input resistance of interneurons at P10 and P20 in mPFC and BC. Two-*
526 *way ANOVA analyses showed a significant effect of age ($F_{(1,27)}$=10.94, p=0.0027) and brain area*
527 *($F_{(1,27)}$=6.65 p=0.0157). Post-hoc analysis showed that the input resistance significantly*

528 *decreased at P20 compared to P10 in mPFC (Tukey's test, p=0.0006) and was significantly higher*
529 *in mPFC compared with BC, at P10 (Tukey's test, p=0.0017), (n=8-9 cells from 5-6 mice/age*
530 *group).*
531 ***(d)*** *Bar graph showing the membrane time constant (τ_m) of interneurons at P10 and P20 in mPFC*
532 *and BC. Two-way ANOVA analyses showed a significant effect of age ($F_{(1,24)}$=14.71, p=0.0008)*
533 *and brain area ($F_{(1,24)}$=6.92 p=0.0147). Post-hoc analysis showed that τ_m was significantly higher*
534 *at P10 compared to P20 in mPFC (Tukey's test, p=0.0006) while it was significantly higher in mPFC*
535 *compared to BC, at P10 (Tukey's test, p=0.0023), (n=8-9 cells from 5-6 mice/age group).*
536 ***(e)*** *Bar graph showing the membrane capacitance (C_m) of interneurons at P10 and P20 in mPFC*
537 *and BC. Two-way ANOVA analyses showed a significant effect between brain areas ($F_{(1,21)}$=6.82,*
538 *p=0.00163) and not between ages ($F_{(1,21)}$=2.60 p=0.1219). Post-hoc analysis showed that Cm was*
539 *significantly higher at P10 compared with P20 in mPFC (Tukey's test, p=0.0291) and was not*
540 *significantly different between mPFC and BC, at P10 (Tukey test, p=0.97) while it was significantly*
541 *higher at P20 in mPFC compared to P20 in BC (Tukey test, p=0.0202), (n=6-9 cells from 5-6*
542 *mice/age group).*
543
544
545 **Decreased PV interneurons in mPFC compared to BC**
546 An additional explanation for the adaptations in inhibitory transmission could come from
547 alterations in interneuron cell densities. To test this, we quantified the number of interneurons
548 per area in cryosections in the mPFC and BC at both ages, in coronal brain slices of Lhx6$^+$-
549 expressing mice. The YFP$^+$ positive cells per area (i.e. Lhx6$^+$ cell density) in mPFC and BC was
550 similar between ages, but was significantly lower in the mPFC, compared to BC (**Figure 7a**).
551 However, we found no contribution of cell death in the mPFC interneuron population, as the
552 percentage of cell death in Lhx6$^+$ neurons is very low in both mPFC and BC in the neonatal group
553 (**Supplementary Figure 2**).
554 The transcription factor Lhx6 is required for the specification and maintenance of main MGE-
555 derived interneurons, PV and SST-positive interneuron subtypes, at postnatal ages (Liodis et al.
556 2007). The neuropeptide SST (both mRNA and protein) is progressively expressed from
557 embryonic to postnatal levels (Bendotti et al. 1990; Forloni et al. 1990). We found that the SST
558 mRNA levels were similar between areas and ages (**Figure 7b**). On the other hand, the
559 emergence of PV immunoreactivity in the mouse cortex shows a delayed development, starting

560 from early postnatal period to adult, with marked area-specific differences(Del Rio et al. 1992).
561 We found that PV was only immunoreactive in BC, and not in mPFC, at P10 (**Figure 7c and**
562 **Supplementary Figure 3**). At P20, PV was immunoreactive in both mPFC and BC, but PV^+ cell
563 density was significantly lower in the mPFC, compared to BC (**Figure 7c**).
564 We also counted the total cell density of mPFC and BC from neonatal and juvenile mice
565 (**Supplementary Figure 4a**) using Nissl staining. In the mPFC, the cell density significantly
566 decreased at P20 compared to P10 (**Supplementary Figure 4b**). On the contrary, in BC, the total
567 cell density significantly increased at P20 compared to P10 (**Supplementary Figure 4b**). When
568 the two brain areas were compared, no difference was found at P10, while the mPFC cell density
569 was significantly lower compared to BC at P20 (**Supplementary Figure 4b**).
570 We further examined whether the alterations in total cell density are derived from alterations
571 in cell density of interneurons by measuring the $Lhx6^+$ neurons over the Nissl-positive cells. No
572 differences were detected between areas and ages (**Supplementary Figure 4c).** These results
573 suggest that the changes in total cell density in mPFC and BC respectively are probably due to
574 changes in other neuronal or glial populations.

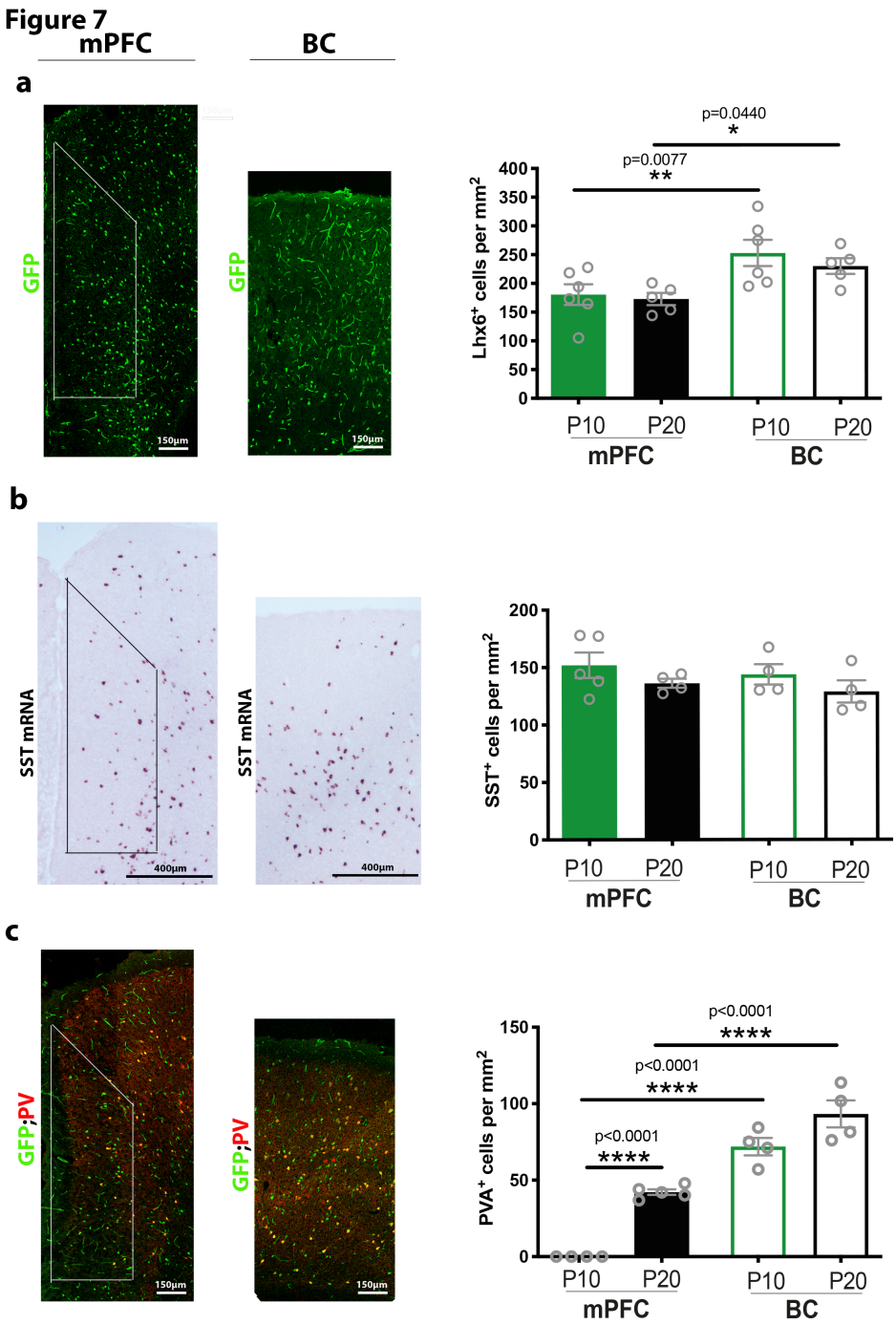

575

576 ***Figure 7. Significant differences in cellular density of Lhx6⁺ interneurons in mPFC and BC at P10***
577 ***and P20.***

578 ***(a)*** *A representative immunostaining with GFP for Lhx6⁺ interneurons in Lhx6-cre;ROSA26fl-*
579 *STOPfl-YFP mice in mPFC and BC at P20 is showing on the left. Scale bars: 150 µm. On the right,*
580 *bar graph comparing Lhx6⁺ interneurons cell density (per mm²) at P10 and P20 in mPFC and BC.*
581 *Two-way ANOVA analyses of the cell density revealed a significant effect of brain area ($F_{(1, 18)}$ =*
582 *13.11, p=0.0020), but not of age ($F_{(1,18)}$=0.7185, p=0.4078). Post-hoc analysis showed that the*

583 *Lhx6$^+$ cell density was not significant different at P20 compared to P10 in mPFC and BC (LSD test,*
584 *p=0.77 and p= 0.38, respectively). The Lhx6$^+$ cell density was significantly lower in mPFC*
585 *compared to BC at P10 and P20, respectively (LSD test, p=0.0077 and p= 0.0440, respectively),*
586 *(P10 in mPFC and BC:n= 5 mice, P20 in mPFC and BC: n=4).*
587 ***(b)*** *A representative in situ hybridization staining for somatostatin positive cells (SST$^+$) using wild*
588 *type animals in mPFC and BC at P20 is showing on the left. Scale bar: 200µm. Bar graph*
589 *comparing cell density based on SST$^+$ expression at P10 and P20 in mPFC and BC. Two-way*
590 *ANOVA analyses of the cell density showed no significant effect of age ($F_{(1, 13)}$= 2.78, p=0.12) and*
591 *brain area ($F_{(1,13)}$=071, p=0.41) was found, (P10 in mPFC: n= 5 mice, P10 in BC and P20 in mPFC*
592 *and BC: n=4).*
593 ***(c)*** *A representative double immunostaining for GFP; PV (PV: parvalbumin) in mPFC and BC at*
594 *P20 is showing on the left. Scale bars: 150 µm. On the right, bar graph comparing cell density*
595 *based on PV$^+$ expression at P10 and P20 in mPFC and BC. Two-way ANOVA analyses of the cell*
596 *density revealed a significant effect of age ($F_{(1, 14)}$ = 45.49, p<0.0001) and brain area ($F_{(1, 14)}$ =*
597 *170.2, p<0.0001). PV$^+$ cells were not found in mPFC but were identified in BC, at P10. Post-hoc*
598 *analysis showed that the PV$^+$ cell density was not significantly different at P20 compared to P10*
599 *in BC (LSD test, p= 0.1089), but was significantly lower in mPFC compared to BC at P20 (LSD test,*
600 *p<0.0001), (P10 and P20 in mPFC: n= 5 mice, P10 and P20 in BC: n=4).*
601
602 **No significant changes in pyramidal neuron excitability between the two brain regions**
603 To determine whether the reduced sEPSC frequency can be explained by changes in pyramidal
604 neuron excitability, we investigated their intrinsic properties. The passive and active properties
605 of pyramidal neurons were measured using current-clamp recordings from layer II/III mPFC and
606 BC. With regards to passive properties, no significant differences were observed in the RMP, the
607 input resistance and the membrane time constant between brain regions and ages
608 (**Supplementary Figure 5, Supplementary Table 1**). Only the membrane capacitance was
609 significantly increased at P20 compared to P10 (**Supplementary Figure 5d, Supplementary Table**
610 **1**), in both brain areas. In addition, the number of spikes generated with increasing current
611 stimulation was not significantly different between ages and regions (**Supplementary Figure 6**).
612 In terms of active properties, the AP amplitude and rate of rise were increased at P20 compared
613 to P10 mPFC, while the AP half-width, rheobase and threshold were not significantly different
614 (**Figure 8, Supplementary Table 1**). The AP amplitude was also significantly increased at P20,

615 compared to P10 in BC, while the other properties did not change (**Figure 8, Supplementary**
616 **Table 1**). Comparing the two regions at the two ages, we found no significant differences of AP
617 properties of pyramidal neurons (**Figure 8, Supplementary Table 1**). The developmental increase
618 of AP amplitude and rate of rise in the mPFC could be due to the on-going maturation of sodium
619 channels in pyramidal neurons. However, these changes could not account for the reduced
620 sEPSCs in the neonatal, compared to juvenile, mPFC and BC.
621

Figure 8

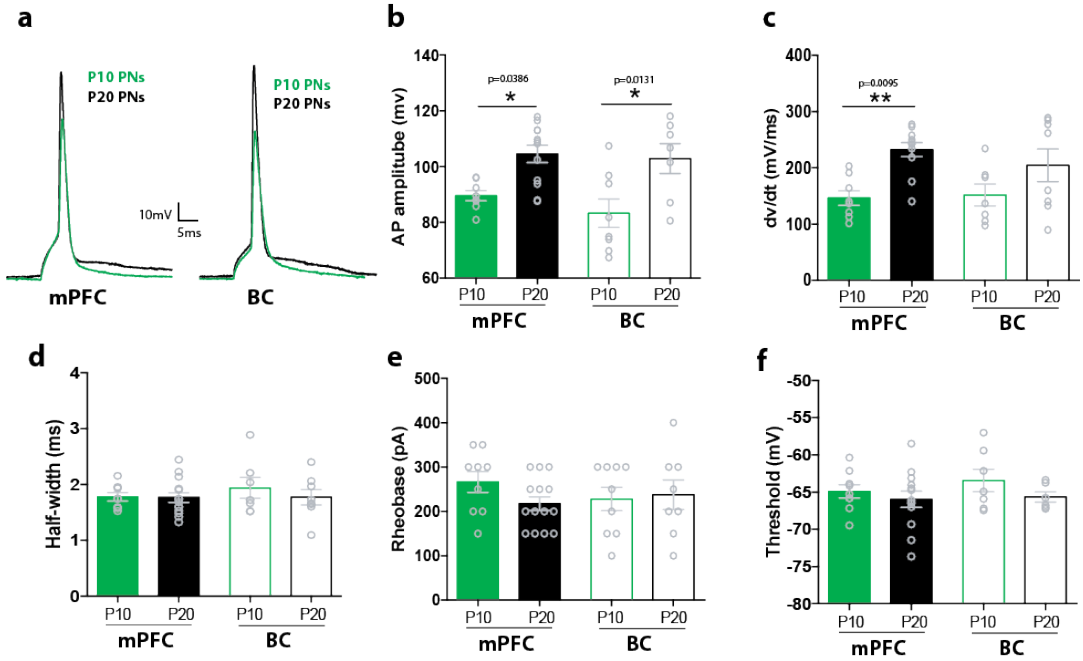

622
623

624 ***Figure 8. Active properties of mPFC and BC pyramidal neurons.***
625 ***(a)*** *Representative traces of action potentials (APs) of layer II/III pyramidal neurons in mPFC*
626 *(left) and BC (right) at P10 (green) and P20 (black), respectively.*
627 ***(b)*** *Bar graph showing the AP amplitude of pyramidal neurons at P10 and P20 in mPFC and BC.*
628 *Two-way ANOVA analyses showed a significant effect of age ($F_{(1, 31)}$ = 18.74, p=0.0001) but not*
629 *on brain area ($F_{(1, 31)}$ = 0.99, p=0.32) was found. Post-hoc analysis showed that the AP amplitude*
630 *significantly increased at P20 compared to P10 in mPFC and BC (Tukey's test, p=0.0386 and p=*
631 *0.0131, respectively) (n=9-14 cells from 6-10 mice/age group).*
632 ***(c)*** *Bar graph showing the AP rate of rise (dv/dt) of pyramidal neuron at P10 and P20 in mPFC*
633 *and BC. Two-way ANOVA analyses showed a significant effect of age ($F_{(1,30)}$= 13.53, p=0.0009)*
634 *but not on brain area ($F_{(1, 30)}$ = 0.36, p=0.55) was found. Post-hoc analysis showed that the AP*

635 *rate of rise significantly increased at P20 compared to P10 in mPFC (Tukey's test, p= 0.0095), but*
636 *not in BC (Tukey's test, p= 0.25) (n=8-14 cells from 6-10 mice/age group).*
637 ***(d)*** *Bar graph showing the AP duration (half-width) of pyramidal neuron at P10 and P20 in mPFC*
638 *and BC. Two-way ANOVA analyses showed no significant effect of age (F(1, 33) = 0.52, p=0.47)*
639 *or brain area ($F_{(1, 33)}$ = 0.43, p=0.51) was found (n=9-14 cells from 6-10 mice/age group).*
640 ***(e)*** *Bar graph showing the AP rheobase of pyramidal neuron at P10 and P20 in mPFC and BC.*
641 *Two-way ANOVA analyses showed no significant effect of age ($F_{(1, 36)}$ = 0.66, p=0.41) or brain*
642 *area ($F_{(1, 36)}$ = 0.16, p=0.69) was found (n=9-14 cells from 6-10 mice/age group).*
643 ***(f)*** *Bar graph showing the AP threshold of pyramidal neuron at P10 and P20 in mPFC and BC.*
644 *Two-way ANOVA analyses showed no significant effect of age ($F_{(1,31)}$ = 1.90, p=0.17) or brain area*
645 *($F_{(1,31)}$=0.55, p=0.46) was found (n=9-14 cells from 6-10 mice/age group).*
646
647 **Effects of mPFC changes in intrinsic and synaptic properties on PFC network activity**
648 In an effort to understand the circuit effects of the aforementioned differences in intrinsic and
649 synaptic properties between neonatal and juvenile mPFC, we adapted an already validated PFC
650 network model (Konstantoudaki et al., 2014) to our current data to generate a neonatal (P10)
651 mPFC model network and juvenile (P20) mPFC model network. Both model networks were
652 stimulated with spontaneous excitatory and inhibitory inputs based on our results for sEPSC and
653 sIPSC frequency and amplitude at both ages (**Figure 1 and Supplementary Table 1**). Our
654 simulation results predict that the intrinsic and synaptic changes from P10 to P20 in mPFC result
655 in enhanced mPFC network activity at P20, compared to P10 (**Figure 9a,e**), as indicated by single-
656 cell activity (**Figure 9a,b**) and the filtered signal (**Figure 9c,d**). Furthermore, we investigated
657 which adaptations have a significant contribution to the network activity properties observed in
658 each model network. Therefore, we generated neonatal (P10) model networks in which the
659 pyramidal model neuron used had P20 properties (N2 network), the fast-spiking interneuron
660 model used had P20 properties (N3 network) or the $GABA_AR$ reversal potential was that of P20
661 (N4 network). We observed that in all the above networks, the resulting neuronal activity
662 generated was significantly reduced compared to the control P10 network (N1) (**Figure 9f**),
663 suggesting that the 'immature' properties of pyramidal neurons, interneurons and $GABA_A$
664 receptors allow the neonatal mPFC network to maintain spontaneous neural activity. Similarly,
665 we generated juvenile model networks in which the pyramidal model neuron used had P10
666 properties (J2 network), the fast-spiking interneuron model used had P10 properties (J3

network) and the $GABA_AR$ reversal potential was that of P10 (J4 network). We find that the resulting neuronal activity generated was significantly increased compared to the control P20 network (J1) (**Figure 9g**). These data support the notion that the maturation of pyramidal neurons and the GABAergic system contributes to restricting network activity in the juvenile mPFC.

Figure 9

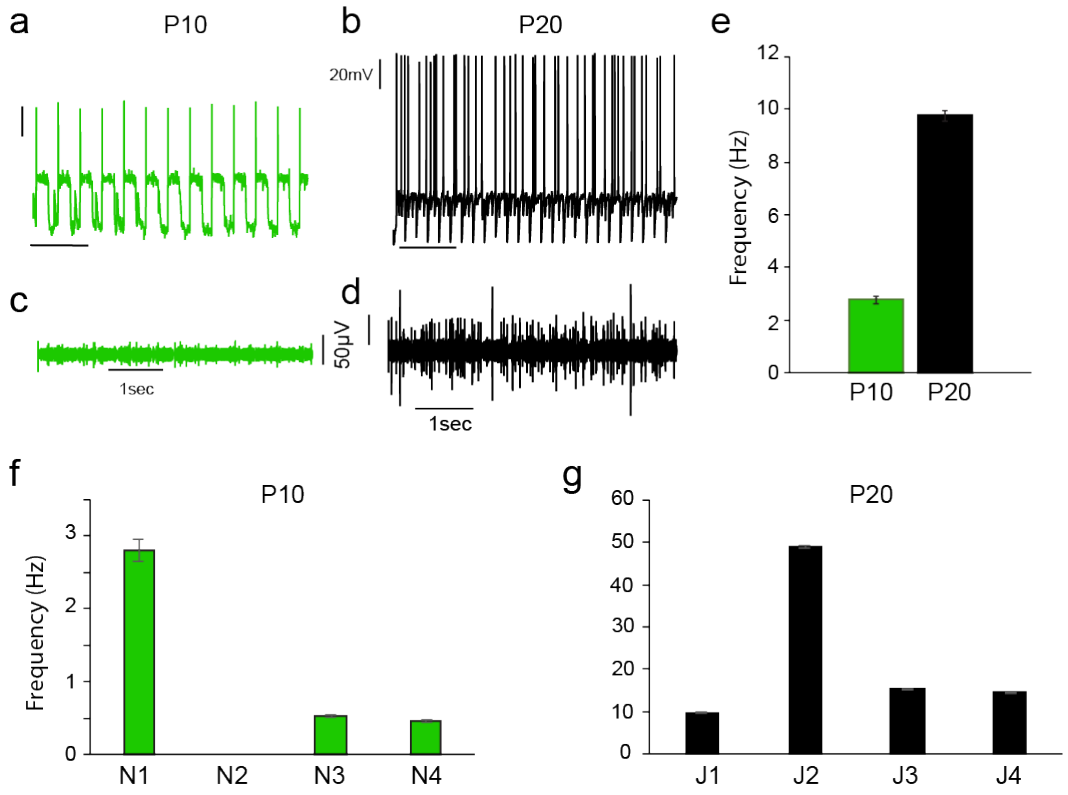

Figure 9. Modeling p10 and p20 PFC network activity

(a,b) *Neuronal response of a single neuron within the PFC model network at p10 and p20*

(c, d) *The filtered voltage response of the p10 and p20 model networks*

(e) *Average frequency of the P10 and P20 model networks.*

(f) *Graph showing how the responses change in modified P10 model networks. N1: control P10 model network, N2: pyramidal model neuron of P20 model network used, N3: fast-spiking interneuron model network of P20 model network used, N4: GABAAR reversal potential was set to -60mV (that of P20 model network).*

(g) *Graph showing how the responses change in modified P20 model networks. J1: control P20 model network, J2: pyramidal model neuron of P10 model network used, J3: fast-spiking*

684 *interneuron model network of P10 model network used, J4: GABAAR reversal potential was set*
685 *to -40mV (that of P10 model network).*
686
687 **Discussion**
688 Our study has identified significant developmental events in the mPFC and the BC between the
689 second and third postnatal weeks. Specifically, we have shown that spontaneous inhibitory
690 transmission, measured as sIPSCs, is increased in mPFC from P10 (neonatal) to P20 (juvenile
691 group). Moreover, our data support a depolarizing action of $GABA_AR$ in the second postnatal
692 week, in the mPFC, as indicated by the presence of non-AMPAR-mediated sEPSCs, depolarizing
693 reversal potential of evoked $GABA_AR$ responses, increased basal fEPSPs following $GABA_AR$
694 activation, which is blocked by concurrent bumetanide application, and decreased protein levels
695 of KCC2. In parallel, differences the intrinsic properties of GABAergic interneurons of mice in the
696 juvenile period resemble are more mature, compared to the neonatal period in mPFC. The above
697 developmental adaptations, along with increased AP amplitude and AP rate-of-rise in pyramidal
698 cells age result in augmented network activity in the juvenile, compared to the neonatal mPFC.
699
700 **Depolarizing action of GABA in the immature cortex**
701 GABA plays a crucial role in inhibiting adult neurons, acting primarily via the chloride-permeable
702 $GABA_AR$ and resulting in hyperpolarization of the membrane potential (Kaila and Voipio 1987).
703 However, GABA action leads to depolarization of immature neurons (i.e. during the first
704 postnatal week in mice), due to an initially higher intracellular chloride concentration $[Cl^-]_{in}$ (Ben-
705 Ari 2001; Ben-Ari et al. 2007; Ben-Ari 2012). The developmental switch of GABA action from
706 depolarizing to hyperpolarizing results from changes in cation-chloride co-transporter
707 expression: NKCC1, a cation-Cl^- importer, is highly expressed in neuronal precursor cells during
708 early brain development (Plotkin et al. 1997; Yamada et al. 2004), while the expression of the
709 K^+-Cl^- cotransporter 2 (KCC2), a cation-Cl^- exporter, increases after the first postnatal week (Ben-
710 Ari 2001; Ben-Ari et al. 2007; Ben-Ari 2012). This increased KCC2 transporter expression might
711 provide a central mechanism for the depolarization to hyperpolarization switch of GABAergic
712 transmission via progressive reduction of $[Cl^-]_{in}$ (Lu et al. 1999; Rivera et al. 1999; Ganguly et al.
713 2001; Ben-Ari 2002; Dzhala et al. 2005; Fiumelli et al. 2005).
714 The $GABA_AR$ switch from depolarizing to hyperpolarizing occurs at P7 in the hippocampus,
715 cortex, amygdala (Ben-Ari et al. 1989; Luhmann and Prince 1991; LoTurco et al. 1995; Owens et

716 al. 1996; Martina et al. 2001; Gulledge and Stuart 2003; Ben-Ari et al. 2007). In the mPFC, GABA
717 application via an iontophoretic pipette and perforated recordings from pyramidal neurons
718 revealed that the reversal potential of GABAA IPSCs is significantly depolarized at P10 and
719 switches around P14 for dendritic IPSCs and after P20 for axon initial segment IPSCs (Rinetti-
720 Viargas et al., 2017). Our results reinforce the $GABA_A$ polarity changes after P10 using perforated
721 IPSC recordings following electrical stimulation in layer II mPFC pyramidal neurons and further
722 supported by decreased levels of KCC2 transporter in the neonatal mPFC. Our results contribute
723 to the more detailed understanding of the protracted maturation of mPFC compared to other
724 cortical areas.
725
726 **Interneurons and mPFC development**
727 Besides the GABAA receptor properties, the number and electrophysiological properties of
728 interneurons change during early development. Our knowledge on the GABAergic interneurons
729 of neonatal mPFC is very limited. PV expression is lowest in juveniles and increases during
730 adolescence to levels similar to those observed in adulthood (Caballero et al. 2014).
731 Furthermore, PV expression is not evident in the neonatal period and emerges during the
732 juvenile period in the mPFC (del Rio et al. 1994; de Lecea et al. 1995; Zheng et al. 2011;
733 Spampanato and Sullivan 2016). Our results agree with these findings, as PV expression was not
734 detected neonatally and was detected in very low amounts during the juvenile period in the
735 mPFC. On the other hand, SST mRNA levels were not altered between the neonatal and juvenile
736 period in the mPFC or the somatosensory cortex.
737 Recordings of $Lhx6^+$- interneurons indicate that both passive and active properties are regulated
738 by age and reach values that better resemble adult MGE-derived interneurons. Specifically, we
739 have found that the input resistance and AP width decrease while the AP rate of rise increases
740 in the mPFC at P20 compared to P10. In part, similar findings have been identified for PV^+ cells
741 in the hippocampus (Doischer et al. 2008; Miyamae et al. 2017) and SST^+ cells in the anterior
742 cingulate cortex (Pan et al. 2017). On the other hand, the AHP amplitude is still quite immature
743 in the mPFC at P20, compared to PV^+, SST^+ interneurons in primary sensory areas or the
744 hippocampus and compared to adult mPFC (Doischer et al. 2008; Yang et al. 2013; Pan et al.
745 2017). Therefore, it is likely that the physiological properties of PV+ and SST+ interneurons in
746 the mPFC continue to change past the third postnatal week.

747 The more mature intrinsic electrophysiological properties of GABAergic interneurons likely
748 contribute to the identified increased frequency of sIPSCs between the second and third
749 postnatal weeks. These results are consistent with the developmental changes of IPSCs in layer
750 III pyramidal neurons of monkey PFC (González-Burgos et al. 2015) and mouse mPFC (Kroon et
751 al. 2019).
752
753 **Pyramidal neurons and network activity**
754 It has been suggested that spontaneous network activity changes from local, highly synchronized
755 to more diffuse from the second to the third postnatal weeks, in the primary sensory cortices
756 (Golshani et al. 2009; Frye and MacLean 2016). In the mPFC, increased levels of network activity
757 have been recorded from P11 to P23 (Bitzenhofer et al., 2021). Our modeling results, which are
758 based on the electrophysiological properties of pyramidal neurons and interneurons we
759 recorded in this study, all reproduce the increased network activity from the neonatal to juvenile
760 ages. A significant contribution to the changes in network activity comes from the changes
761 observed in pyramidal neurons, in particular, the developmental increase of AP amplitude and
762 rate of rise, which could be due to the on-going maturation of sodium channels in pyramidal
763 neurons.
764 Studies in developing mPFC pyramidal neurons have proposed that there is a unique sensitive
765 time window for synaptic maturation of these neurons from individual cortical layers. During rat
766 mPFC layer V development, the intrinsic properties, synaptic inputs and morphology of
767 pyramidal neurons develop together during early postnatal life. While the greatest changes were
768 reported during the first ten days after birth, the adult-like properties emerged after the end of
769 the third week (P21) (Zhang et al. 2011). This study confirms that the second postnatal week is
770 a period of rapid growth, similar to that in other neocortical regions by combining functional and
771 structural measurements of developing pyramidal neurons in mouse mPFC (Zhu 2000; Romand
772 et al. 2011).
773 **Developmental PFC malformations lead to cognitive disorders in adulthood**
774 The neonatal functional maturation of GABAergic circuits and E/I (excitation to inhibition)
775 balance are critical for PFC-dependent behaviours and plasticity in the adult while their
776 malfunction leads to many psychiatric disorders (Benes 1991; Kilb 2012; Ferguson and Gao
777 2018). From the prenatal period to late adolescence, the PFC network is highly vulnerable to
778 genetic and environmental factors (Andersen 2003), since the mPFC is one of the latest cortical

779 regions to develop (Huttenlocher 1990). While many studies have focused on understanding
780 several developmental processes during adolescence (Caballero et al. 2016), our knowledge
781 regarding the ongoing cellular and network developmental processes during the perinatal period
782 is notably limited, despite significant evidence showing that environmental manipulations
783 during this period manifest as complex psychiatric and neurologic disorders in adulthood
784 (Weinberger 1986).
785 The delayed developmental shift of GABA action in various mouse models mimicking human
786 brain disorders have been investigated, including the maternal immune activation model
787 (Corradini et al. 2018; Fernandez et al. 2018), the Scn1a and Scn1b mouse models of Dravet
788 syndrome (Yuan et al., 2019), the 22q11.2 deletion syndrome (Amin et al. 2017) and the Fmr1
789 deficient model of fragile X syndrome (He et al. 2018). In the latter study, early postnatal
790 correction of GABA depolarization (bumetanide-treated) led to sufficient normalization of the
791 mature BC network (He et al. 2018). Therefore, the NKCC1 and KCC2 chloride transporters have
792 been proposed as a potential therapeutic target of epilepsies by many studies in animal models
793 and human patients (Moore et al. 2017).
794 Our study focuses in understanding the early developmental cellular and physiological
795 mechanisms of mPFC circuits, before adolescence, and proposes that the neonatal mPFC
796 compared to BC exhibits a delayed switch from depolarization to hyperpolarization function of
797 $GABA_AR$. Our results raise the possibility that the delayed maturation of mPFC compared to other
798 cortical areas depends on a combination of a delayed switch from depolarization to
799 hyperpolarization function of the $GABA_AR$ and delayed maturation of interneurons.
800

801 **Acknowledgements:**

802 Authors are grateful to Emmanuella Foinikianaki for her help with Matlab analysis and histology
803 and to Giasemi Eptaminitaki for her help in *in situ* hybridization experiments. They also would
804 like to thank all the members of Karagogeos and Sidiropoulou Labs and the animal facility of the
805 IMBB for help with experiments.

806 This study was co-financed through the Operational Program "Education and Lifelong Learning"
807 of the National Strategic Reference Framework – Research Funding Program (EDBM34) by a
808 grant to DK (10040) and through the BIOIMAGING-GR, National Roadmap for Research
809 Infrastructures from the European Union (European Social Fund-ESF) and Greek National Funds.

KK has been a recipient of the Manasaki fellowship and a Medical School fellowship of the University of Crete and a poster award at the 27th Hellenic Society for Neuroscience Meeting.

Author Contributions:

All experiments were conceived and designed by K.K., K.S., and D.K. All experiments performed by K.K., A.V., and O.C. Computational simulations were performed by K.S. Data were analyzed by K.K., A.V., O.C., M.D. K.S. and discussed with D.K. Manuscript was written by K.K., D.K. and K.S. All authors discussed and commented on the manuscript.

References:

Allene C, Cattani A, Ackman JB, Bonifazi P, Aniksztejn L, Ben-Ari Y, Cossart R. 2008. Sequential Generation of Two Distinct Synapse-Driven Network Patterns in Developing Neocortex. J Neurosci. 28:12851–12863.

Amin H, Marinaro F, De Pietri Tonelli D, Berdondini L. 2017. Developmental excitatory-to-inhibitory GABA-polarity switch is disrupted in 22q11.2 deletion syndrome: a potential target for clinical therapeutics. Scientific Reports. 1–18.

Andersen SL. 2003. Trajectories of brain development: point of vulnerability or window of opportunity? Neuroscience & Biobehavioral Reviews. 27:3–18.

Bahrey HLP, Moody WJ. 2003. Early Development of Voltage-Gated Ion Currents and Firing Properties in Neurons of the Mouse Cerebral Cortex. Journal of Neurophysiology. 89:1761–1773.

Bartolini G, Ciceri G, Marin O. 2013. Integration of GABAergic Interneurons into Cortical Cell Assemblies: Lessons from Embryos and Adults. 79:849–864.

Ben-Ari Y. 2001. Developing networks play a similar melody. Trends in Neurosciences. 24:353–360.

Ben-Ari Y. 2002. Excitatory actions of gaba during development: the nature of the nurture. Nat Rev Neurosci. 3:728–739.

Ben-Ari Y. 2012. Refuting the challenges of the developmental shift of polarity of GABA actions: GABA more exciting than ever! 1–18.

838 Ben-Ari Y, Cherubini E, Corradetti R, Gaiarsa JL. 1989. Giant synaptic potentials in immature rat
839 CA3 hippocampal neurones. The Journal of Physiology. 416:303–325.
840 Ben-Ari Y, Gaiarsa JL, Tyzio R, Khazipov R. 2007. GABA: A Pioneer Transmitter That Excites
841 Immature Neurons and Generates Primitive Oscillations. Physiological Reviews. 87:1215–
842 1284.
843 Ben-Ari Y, Khalilov I, Kahle KT, Cherubini E. 2012. The GABA Excitatory/Inhibitory Shift in Brain
844 Maturation and Neurological Disorders. The Neuroscientist. 18:467–486.
845 Bendotti C, Hohmann C, Forloni G, Brain RRD, 1990. 1990. Developmental expression of
846 somatostatin in mouse brain. II. In situ hybridization. Elsevier. 53:26–39.
847 Benes FM. 1991. Deficits in Small Interneurons in Prefrontal and Cingulate Cortices of
848 Schizophrenic and Schizoaffective Patients. Archives of General Psychiatry. 48:996–1001.
849 Best JR, Miller PH. 2010. A Developmental Perspective on Executive Function. Child
850 Development. 81:1641–1660.
851 Bitzenhofer SH, Ahlbeck J, Wolff A, Wiegert JS, Gee CE, Oertner TG, Hanganu-Opatz IL. 2017.
852 Layer-specific optogenetic activation of pyramidal neurons causes beta-gamma entrainment
853 of neonatal networks. Nature Communications. 8:14563.
854 Bitzenhofer SH, Pöpplau JA, Chini M, Marquardt A, Hanganu-Opatz IL. A transient developmental
855 increase in prefrontal activity alters network maturation and causes cognitive dysfunction
856 in adult mice. Neuron. 2021 Apr 21;109(8):1350-1364.e6.
857 Bitzenhofer SH, Sieben K, Siebert KD, Spehr M, Hanganu-Opatz IL. 2015. Oscillatory Activity in
858 Developing Prefrontal Networks Results from Theta-Gamma-Modulated Synaptic Inputs.
859 CellReports. 11:486–497.
860 Brockmann MD, Pöschel B, Cichon N, Hanganu-Opatz IL. 2011. Coupled Oscillations Mediate
861 Directed Interactions between Prefrontal Cortex and Hippocampus of the Neonatal Rat.
862 Neuron. 71:332–347.
863 Burgard EC, Hablitz JJ. 1993. Developmental changes in NMDA and non-NMDA receptor-
864 mediated synaptic potentials in rat neocortex. Journal of Neurophysiology. 69:230–240.
865 Caballero A, Flores-Barrera E, Cass DK, Tseng KY. 2014. Differential regulation of parvalbumin
866 and calretinin interneurons in the prefrontal cortex during adolescence. Brain Struct Funct.
867 219:395–406.
868 Caballero A, Granberg R, Tseng KY. 2016. Mechanisms contributing to prefrontal cortex
869 maturation during adolescence. Neuroscience & Biobehavioral Reviews. 1–29.

870 Casey BJ, Giedd JN, Thomas KM. 2000. Structural and functional brain development and its
871 relation to cognitive development. Biological Psychology. 54:241–257.
872 Chalkiadaki K, Velli A, Kyriazidis E, Stavroulaki V, Vouvoutsis V, Chatzaki E, Aivaliotis M,
873 Sidiropoulou K. 2019. Development of the MAM model of schizophrenia in mice: Sex
874 similarities and differences of hippocampal and prefrontal cortical function.
875 Neuropharmacology 144, 193–207.
876 Chini, M. & Hanganu-Opatz, I. L. 2020. Prefrontal Cortex Development in Health and Disease:
877 Lessons from Rodents and Humans. *Trends Neurosci*
878 Clancy B, Darlington RB, Neuroscience BF, 2001. 2001. Translating developmental time across
879 mammalian species. Elsevier. 105:7–17.
880 Corradini I, Focchi E, Rasile M, Morini R, Desiato G, Tomasoni R, Lizier M, Ghirardini E, Fesce R,
881 Morone D, Barajon I, Antonucci F, Pozzi D, Matteoli M. 2018. Maternal Immune Activation
882 Delays Excitatory-to-Inhibitory Gamma-Aminobutyric Acid Switch in Offspring. Biological
883 Psychiatry. 83:680–691.
884 de Lecea L, del Ri o JA, Soriano E. 1995. Developmental expression of parvalbumin mRNA in the
885 cerebral cortex and hippocampus of the rat. Molecular Brain Research. 32:1–13.
886 DeFelipe J, Fariñas I. 1992. The pyramidal neuron of the cerebral cortex: Morphological and
887 chemical characteristics of the synaptic inputs. Progress in Neurobiology. 39:563–607.
888 del Rio J, De Lecea L, Ferrer I, Soriano E. 1994. The development of parvalbumin-
889 immunoreactivity in the neocortex of the mouse. 81:247–259.
890 Del Rio JA, Soriano E, Ferrer I. 1992. Development of GABA-immunoreactivity in the neocortex
891 of the mouse. J Comp Neurol. 326:501–526.
892 Diamond A. 2005. Normal Development of Prefrontal Cortex from Birth to Young Adulthood:
893 Cognitive Functions, Anatomy, and Biochemistry. In: Principles of Frontal Lobe Function.
894 Oxford University Press. p. 466–503.
895 Doischer D, Aurel Hosp J, Yanagawa Y, Obata K, Jonas P, Vida I, Bartos M. 2008. Postnatal
896 Differentiation of Basket Cells from Slow to Fast Signaling Devices. J Neurosci. 28:12956–
897 12968.
898 Dzhala VI, Talos DM, Sdrulla DA, Brumback AC, Mathews GC, Benke TA, Delpire E, Jensen FE,
899 Staley KJ. 2005. NKCC1 transporter facilitates seizures in the developing brain. Nature
900 Medicine 2005 11:11. 11:1205–1213.

901 Ferguson BR, Gao W-J. 2018. PV Interneurons: Critical Regulators of E/I Balance for Prefrontal
902 Cortex-Dependent Behavior and Psychiatric Disorders. Front Neural Circuits. 12:479–13.
903 Fernandez A, Dumon C, Guimond D, Tyzio R, Bonifazi P, Lozovaya N, Burnashev N, Ferrari DC,
904 Ben-Ari Y. 2018. The GABA Developmental Shift Is Abolished by Maternal Immune Activation
905 Already at Birth. Cerebral Cortex. 130:e1447–11.
906 Fiumelli H, Cancedda L, Poo M-M. 2005. Modulation of GABAergic Transmission by Activity via
907 Postsynaptic Ca2+-Dependent Regulation of KCC2 Function. Neuron. 48:773–786.
908 Forloni G, Hohmann C, Research JCDB, 1990. 1990. Developmental expression of somatostatin
909 in mouse brain. I. Immunocytochemical studies. Elsevier. 53:6–25.
910 Frye CG, MacLean JN. 2016. Spontaneous activations follow a common developmental course
911 across primary sensory areas in mouse neocortex. Journal of Neurophysiology. 116:431–
912 437.
913 Fuster J. 2015. The Prefrontal Cortex. Academic Press.
914 Ganguly K, Schinder AF, Wong ST, Poo M-M. 2001. GABA Itself Promotes the Developmental
915 Switch of Neuronal GABAergic Responses from Excitation to Inhibition. Cell. 105:521–532.
916 Golshani P, Goncalves JT, Khoshkhoo S, Mostany R, Smirnakis S, Portera-Cailliau C. 2009.
917 Internally Mediated Developmental Desynchronization of Neocortical Network Activity. J
918 Neurosci. 29:10890–10899.
919 González-Burgos G, Miyamae T, Pafundo DE, Yoshino H, Rotaru DC, Hoftman G, Datta D, Zhang
920 Y, Hammond M, Sampson AR, Fish KN, Bard Ermentrout G, Lewis DA. 2015. Functional
921 Maturation of GABA Synapses During Postnatal Development of the Monkey Dorsolateral
922 Prefrontal Cortex. Cerebral Cortex. 25:4076–4093.
923 Gulledge AT, Stuart GJ. 2003. Excitatory Actions of GABA in the Cortex. Neuron. 37:299–309.
924 Guo ZV, Li N, Huber D, Ophir E, Gutnisky D, Ting JT, Feng G, Svoboda K. 2014. Flow of Cortical
925 Activity Underlying a Tactile Decision in Mice. Neuron. 81:179–194.
926 He Q, Arroyo ED, Smukowski SN, Xu J, Piochon C, Savas JN, Portera-Cailliau C, Contractor A. 2018.
927 Critical period inhibition of NKCC1 rectifies synapse plasticity in the somatosensory cortex
928 and restores adult tactile response maps in fragile X mice. Mol Psychiatry. 8:109–116.
929 Heidbreder CA, Groenewegen HJ. 2003. The medial prefrontal cortex in the rat: evidence for a
930 dorso-ventral distinction based upon functional and anatomical characteristics.
931 Neuroscience & Biobehavioral Reviews. 27:555–579.
932 Hensch TK. 2016. The Power of the Infant Brain. Nature Publishing Group. 314:64–69.

933 Huguenard JR, Hamill OP, Prince DA. 1988. Developmental changes in Na+ conductances in rat
934 neocortical neurons: appearance of a slowly inactivating component. Journal of
935 Neurophysiology. 59:778–795.
936 Huttenlocher PR. 1990. Morphometric study of human cerebral cortex development.
937 Neuropsychologia. 28:517–527.
938 Kaila K, Voipio J. 1987. Postsynaptic fall in intracellular p H induced by GABA-activated
939 bicarbonate conductance. Nature. 330:163–165.
940 Khazipov R, Luhmann HJ. 2006. Early patterns of electrical activity in the developing cerebral
941 cortex of humans and rodents. Trends in Neurosciences. 29:414–418.
942 Khazipov R, Minlebaev M, Valeeva G. 2013. Early gamma oscillations. Neuroscience. 250:240–
943 252.
944 Khazipov R, Sirota A, Leinekugel X, Holmes GL, Ben-Ari Y, Buzsáki G. 2004. Early motor activity
945 drives spindle bursts in the developing somatosensory cortex. Nature. 432:758–761.
946 Kilb W. 2012. Development of the GABAergic System from Birth to Adolescence. The
947 Neuroscientist. 18:613–630.
948 Kirmse K, Kummer M, Kovalchuk Y, Witte OW, Garaschuk O, Holthoff K. 2015. GABA depolarizes
949 immature neurons and inhibits network activity in the neonatal neocortex in vivo. Nature
950 Communications. 6:7750.
951 Kolb B, Mychasiuk R, Muhammad A, Li Y, Frost DO, Gibb R. 2012. Experience and the developing
952 prefrontal cortex. Proc Natl Acad Sci USA. 109:17186–17193.
953 Konstantoudaki X, Papoutsi A, Chalkiadaki K, Poirazi P, Sidiropoulou K. Modulatory effects of
954 inhibition on persistent activity in a cortical microcircuit model. Front Neural Circuits. 2014
955 Jan 31;8:7.
956 Konstantoudaki X, Chalkiadaki K, Tivodar S, Karagogeos D, Sidiropoulou K. 2016. Impaired
957 synaptic plasticity in the prefrontal cortex of mice with developmentally decreased number
958 of interneurons. Neuroscience. 1–13.
959 Kriegstein AR, Suppes T, Prince DA. 1987. Cellular and synaptic physiology and epileptogenesis
960 of developing rat neocortical neurons in vitro. Developmental Brain Research. 34:161–171.
961 Kroeze Y, Oti M, van Beusekom E, Cooijmans RHM, van Bokhoven H, Kolk SM, Homberg JR, Zhou
962 H. 2017. Transcriptome Analysis Identifies Multifaceted Regulatory Mechanisms Dictating a
963 Genetic Switch from Neuronal Network Establishment to Maintenance During Postnatal
964 Prefrontal Cortex Development. Cerebral Cortex. 1–19.

965 Kroon T, van Hugte E, van Linge L, Mansvelder HD, Meredith RM. 2019. Early postnatal
966 development of pyramidal neurons across layers of the mouse medial prefrontal cortex.
967 Scientific Reports. 9:5037–16.
968 Le Magueresse C, Monyer H. 2013. GABAergic Interneurons Shape the Functional Maturation of
969 the Cortex. Neuron. 77:388–405.
970 Liodis P, Denaxa M, Grigoriou M, Akufo-Addo C, Yanagawa Y, Pachnis V. 2007. Lhx6 Activity Is
971 Required for the Normal Migration and Specification of Cortical Interneuron Subtypes.
972 Journal of Neuroscience. 27:3078–3089.
973 LoTurco JJ, Owens DF, Heath MJS, Davis MBE, Kriegstein AR. 1995. GABA and glutamate
974 depolarize cortical progenitor cells and inhibit DNA synthesis. Neuron. 15:1287–1298.
975 Lu J, Karadsheh M, Delpire E. 1999. Developmental regulation of the neuronal-specific isoform
976 of K-CL cotransporter KCC2 in postnatal rat brains. J Neurobiol. 39:558–568.
977 Luhmann HJ, Prince DA. 1991. Postnatal maturation of the GABAergic system in rat neocortex.
978 Journal of Neurophysiology. 65:247–263.
979 Martina M, Royer S, Paré D. 2001. Cell-Type-Specific GABA Responses and Chloride Homeostasis
980 in the Cortex and Amygdala. Journal of Neurophysiology. 86:2887–2895.
981 McCormick DA, Prince DA. 1987. Post-natal development of electrophysiological properties of
982 rat cerebral cortical pyramidal neurones. The Journal of Physiology. 393:743–762.
983 Miyamae T, Chen K, Lewis DA, González-Burgos G. 2017. Distinct physiological maturation of
984 parvalbumin-positive neuron subtypes in mouse prefrontal cortex. J Neurosci. 3325–16–48.
985 Moore YE, Kelley MR, Brandon NJ, Deeb TZ, Moss SJ. 2017. Seizing Control of KCC2: A New
986 Therapeutic Target for Epilepsy. Trends in Neurosciences. 40:555–571.
987 Mòdol L, Bollmann Y, Tressard T, Baude A, Che A, Duan ZRS, Babij R, De Marco García NV, Cossart
988 R. 2019. Assemblies of Perisomatic GABAergic Neurons in the Developing Barrel Cortex.
989 Neuron. 1–18.
990 Owens DF, Boyce LH, Davis MBE, Kriegstein AR. 1996. Excitatory GABA Responses in Embryonic
991 and Neonatal Cortical Slices Demonstrated by Gramicidin Perforated-Patch Recordings and
992 Calcium Imaging. J Neurosci. 16:6414–6423.
993 Pan G, Yang J-M, Hu X-Y, Li X-M. 2017. Postnatal development of the electrophysiological
994 properties of somatostatin interneurons in the anterior cingulate cortex of mice. Nature
995 Publishing Group. 1–12.

996 Plotkin MD, Snyder EY, Hebert SC, Delpire E. 1997. Expression of the Na-K-2Cl cotransporter is
997 developmentally regulated in postnatal rat brains: A possible mechanism underlying GABA's
998 excitatory role in immature brain. J Neurobiol. 33:781–795.
999 Ramoa AS, McCormick DA. 1994. Developmental changes in electrophysiological properties of
1000 LGNd neurons during reorganization of retinogeniculate connections. J Neurosci. 14:2089–
1001 2097.
1002 Rinetti-Vargas, Gina, Khanhky Phamluong, Dorit Ron, and Kevin J. Bender. 2017. "Periadolescent
1003 Maturation of GABAergic Hyperpolarization at the Axon Initial Segment." *CellReports*
1004 20(1):21–29.
1005 Rivera C, Voipio J, Payne JA, Ruusuvuori E, Lahtinen H, Lamsa K, Pirvola U, Saarma M, Kaila K.
1006 1999. The K+/Cl- co-transporter KCC2 renders GABA hyperpolarizing during neuronal
1007 maturation. Nature. 397:251–255.
1008 Romand S, Wang Y, Toledo-Rodriguez M, Markram H. 2011. Morphological Development of
1009 Thick-Tufted Layer V Pyramidal Cells in the Rat Somatosensory Cortex. Front Neuroanat. 5.
1010 Rossant C, Kadir SN, Goodman DFM, et al. Spike sorting for large, dense electrode arrays. *Nat*
1011 *Neurosci*. 2016;19(4):634-641. doi:10.1038/nn.4268
1012 Schaeren-Wiemers N, Gerfin-Moser A. 1993. A single protocol to detect transcripts of various
1013 types and expression levels in neural tissue and cultured cells: in situ hybridization using
1014 digoxigenin-labelled cRNA probes. Histochemistry. 100:431–440.
1015 Schubert D, Martens GJM, Kolk SM. 2014. Molecular underpinnings of prefrontal cortex
1016 development in rodents provide insights into the etiology of neurodevelopmental disorders.
1017 20:795–809.
1018 Southwell DG, Paredes MF, Galvao RP, Jones DL, Froemke RC, Sebe JY, Alfaro-Cervello C, Tang Y,
1019 García-Verdugo JM, Rubenstein JL, Baraban SC, Alvarez-Buylla A. 2012. Intrinsically
1020 determined cell death of developing cortical interneurons. Nature. 491:109–113.
1021 Spampanato J, Sullivan R. 2016. Development and physiology of GABAergic feedback excitation
1022 in parvalbumin expressing interneurons of the mouse basolateral amygdala. Physiological
1023 Reports, 4:e12664–15.
1024 Tsujimoto S. 2008. The prefrontal cortex: functional neural development during early childhood.
1025 The Neuroscientist. 14:345–358.

1026 Van De Werd HJJM, Rajkowska G, Evers P, Uylings HBM. 2010. Cytoarchitectonic and
1027 chemoarchitectonic characterization of the prefrontal cortical areas in the mouse. Brain
1028 Struct Funct. 214:339–353.
1029 Vidaki M, Tivodar S, Doulgeraki K, Tybulewicz V, Kessaris N, Pachnis V, Karagogeos D. Rac1-
1030 dependent cell cycle exit of MGE precursors and GABAergic interneuron migration to the
1031 cortex. Cereb Cortex. 2012 Mar;22(3):680-92.
1032 Weinberger DR. 1986. Physiologic Dysfunction of Dorsolateral Prefrontal Cortex in
1033 Schizophrenia. Archives of General Psychiatry. 43:114.
1034 Yamada J, Okabe A, Toyoda H, Kilb W, Luhmann HJ, Fukuda A. 2004. Cl− uptake promoting
1035 depolarizing GABA actions in immature rat neocortical neurones is mediated by NKCC1. The
1036 Journal of Physiology. 557:829–841.
1037 Yang JM, Zhang J, Yu YQ, Duan S, Li XM. 2013. Postnatal Development of 2 Microcircuits Involving
1038 Fast-Spiking Interneurons in the Mouse Prefrontal Cortex. Cerebral Cortex. 24:98–109.
1039 Yuan Y, Malley HAOX, Smaldino MA, Bouza AA, Hull JM, Isom LL. 2019. Delayed maturation of
1040 GABAergic signaling in the Scn1a and Scn1b mouse models of Dravet Syndrome. Scientific
1041 Reports. 1–16.
1042 Zhang Z, Jiao Y-Y, Sun Q-Q. 2011. Developmental maturation of excitation and inhibition balance
1043 in principal neurons across four layers of somatosensory cortex. Neuroscience. 174:10–25.
1044 Zheng K, An JJ, Yang F, Xu W. 2011. TrkB signaling in parvalbumin-positive interneurons is critical
1045 for gamma-band network synchronization in hippocampus. Proc Natl Acad Sci USA; 108
1046 (41):17201-17206;
1047 Zhu JJ. 2000. Maturation of layer 5 neocortical pyramidal neurons: amplifying salient layer 1 and
1048 layer 4 inputs by Ca2+ action potentials in adult rat tuft dendrites. The Journal of Physiology.
1049 526:571–587.
1050
1051